Received: 29 December 2020 | Revised: 2 February 2021 | Accepted: 3 February 2021

DOI: 10.1002/nano.202000309

nano select Open Access WILEY

REVIEW

# Progress and biomedical applications of MXenes

**Jing Huang**[1,2] | **Zhe Li**[2,3] | **Yukun Mao**[4] | **Zhou Li**[1,2,5]

[1] Center on Nanoenergy Research, College of chemistry and chemical engineering, Guangxi University, Nanning, China

[2] CAS Center for Excellence in Nanoscience, Beijing Key Laboratory of Micro-Nano Energy and Sensor, Beijing Institute of Nanoenergy and Nanosystems, Chinese Academy of Sciences, Beijing, China

[3] Institute of Engineering Medicine, School of Life Science, Beijing Institute of Technology, Beijing, China

[4] Department of Orthopedics, Zhongnan Hospital of Wuhan University, Wuhan, Hubei, China

[5] School of Nanoscience and Technology, University of Chinese Academy of Sciences, Beijing, China

**Correspondence**
Zhou Li, Center on Nanoenergy Research, College of chemistry and chemical engineering, Guangxi University, Nanning 530004, China.
Email: zli@binn.cas.cn

**Funding information**
National Natural Science Foundation of China, Grant/Award Number: 61875015; Science and Technology Planning Project of Guangdong Province, Grant/Award Number: 2018B030331001; Beijing Natural Science Foundation, Grant/Award Number: JQ20038; National Youth Talent Support Program; Fundamental Research Funds for the Central Universities

**Abstract**

As a new kind of two-dimensional material, MXene is first discovered in 2011. Because of its diverse chemical composition with excellent physical and chemical properties, the family of MXenes has attracted people's extensive research interest in various fields, such as energy storage, environment, catalysis and biomedical applications, among which the researches about biomedical applications are relatively more burgeoning than that in other fields. This review concludes the progress and biomedical applications of MXenes. Firstly, the development background of MXenes is introduced. Then, the synthesis methods, structures and properties, surface modification strategies, biomedical applications, cytotoxicity and biocompatibility of MXenes are demonstrated in each chapter successively. At last, the materials of MXenes are summarized, besides, the opportunities and challenges faced by MXenes in the future are prospected. This review will provide some help for the advancement and application of MXenes.

**KEYWORDS**
bioimaging, biosensing, MXene, therapeutic, tissue engineering

## 1 | INTRODUCTION

Recently, because of their ultra-thin structure and excellent performance, 2D nanomaterials have been used in many and various fields widely, like energy storage,[1–4] catalysis,[5–7] smart wearable sensors[8–11] and biomedical applications.[12–15] As an emerging branch of the 2D material family, MXenes, which are first discovered by Professor Yury Gogotsi and Professor Michel W. Barsoum with their colleagues in Drexel University in 2011, have attracted extensive attention in various research fields because of their atomic layer thickness and various excellent properties, such as semiconductor properties, surface hydrophilic properties, magnetic properties, rich surface functional groups, and so on. MXene is etched from its parent MAX phase, of which formula is $M_{n+1}X_nT_x$

("M" denotes the transition metals, "X" denotes C and/or N elements, "$T_x$" denotes the surface termination groups such as -O, –F and –OH, and n = 1–3. "A" denotes the elements of group IIIA/IVA). The first MXene, $Ti_3C_2T_x$, was obtained via etching Al atomic layer from $Ti_3AlC_2$.[16] Due to the diversity of element composition, up to now, over 30 kinds of MXenes compositions have been synthesized through experiments, and more than dozens of MXenes have been predicted theoretically, which expands the family of MXenes. MXenes can be used as magnetic shielding material, electrode material, conductive thin film material, capacitor material, electrocatalyst and so on because of their rich surface functional groups, outstanding electrical and optical properties, extraordinary mechanical and magnetic properties. Besides, owing to the abundant surface functional groups, MXenes can be modified with all kinds of material to enhance their properties and expand their application.

With the rapid development of biomedicine and the attractive physiochemical properties of two-dimensional materials, many researchers have focused on the biomedical applications of two-dimensional materials, such as hexagonal boron nitrides (h-BN), graphene and its derivatives, transition metal oxides (TMOs), layered double hydroxides (LDHs) and MXenes. Compared with other 2D materials, MXenes possess abundant functional groups on their surface which makes modification more flexible. What's more, MXenes contain complete metal atomic layers and tunable composition as well as hydrophilicity, the combination of these properties makes them ideal for biomedical applications. Also, the cost-effective scale-up production of MXenes maybe a superiority. So far, the main applications of MXenes in biomedical field include bioimaging, antibacterial, biosensing, drug delivery, tissue engineering, and various therapeutic methods (Figure 1). For example, MXenes have strong light absorption and conversion ability in near infrared, so they can be used for tumor ablation, which is called photothermal therapy that can reach deep in tissues of the bodies, be specific to cancer cells, and has less harm to human body. In addition, as contrast agents, tumor location can be monitored in real-time through bioimaging while treating cancer. In addition, the modified MXenes can also carry anticancer drugs and release drugs in a targeted manner. So far, the synergistic treatment of photothermal therapy and chemotherapy as well as the real-time monitoring of bioimaging have greatly improved the effectiveness of cancer treatment. What's more, MXenes are expected to be candidate materials for manufacturing biocompatible equipment to detect biological events quickly and easily. The other biomedical applications of MXenes will be discussed in this review in later chapters.

In a word, this paper will summarize the structure, performance, modification, biomedical application and cytotoxicity evaluation of MXenes, and put forward some views on their future work in biomedical field.

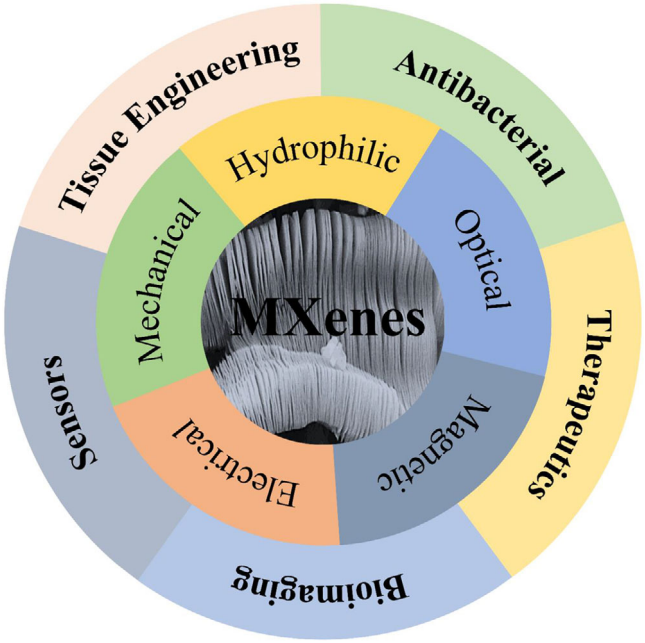


**FIGURE 1** The properties and biomedical applications of MXenes are summarized. Reproduced with permission.[17] Copyright 2012, American Chemical Society

## 2 | SYNTHESIS OF MXENES

Over the past few years, the synthetic methods of MXenes have been developed so fast for making more and new species of MXenes. Overall, the methods can be divided into two categories in which the one is top-down method and another is bottom-up method. The former is commonly used while the latter is not commonly used in making MXenes. Next, we will discuss these two methods specifically.

### 2.1 | Top-down method

Compared with the bottom-up method, the top-down method is used a lot. Generally, the MXenes are obtained via selectively etching the Al layers from the MAX phases and then exfoliating them in these top-down methods (Figure 2A). Usually, the MAX phase precursors are relatively large, so these methods will be operated more easily than those bottom-up methods. According to etching method, they can be divided into HF etching method, bifluoride ($NH_4HF_2$) method, LiF/HCl etching method, molten salt etching, and minimally intensive layer delamination (MILD) etching method. For example, Yury Gogotsi et al. synthesized the first MXene ($Ti_3C_2T_x$)

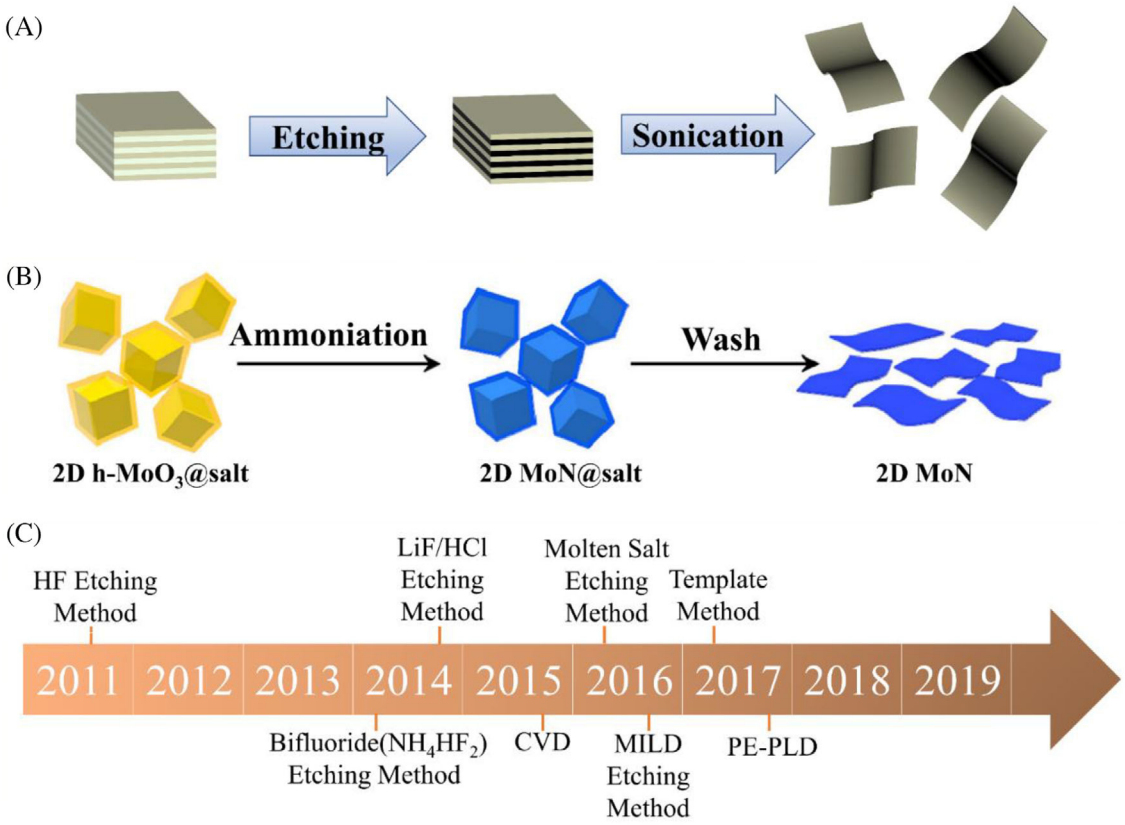


**FIGURE 2** A, The etching synthesis of MXenes from MAX phases. B, Synthesis of 2D MoN by template method. Reproduced with permission.[33] Copyright 2017, American Chemical Society. C, So far, the synthesis methods of MXenes and the year of the corresponding first article

by immersing $Ti_3AlC_2$ in HF in Drexel University.[16] And the reactions can be concluded as follows:

$$Ti_3AlC + 3HF = AlF_3 + 3/2H_2 + Ti_3C_2 \quad (1)$$

$$Ti_3C_2 + 2H_2O = Ti_3C_2(OH)_2 + H_2 \quad (2)$$

$$Ti_3C_2 + 2HF = Ti_3C_2F_2 + H_2 \quad (3)$$

However, the HF is harmful to both environment and human body, moreover, this kind of method will make the performance of MXenes low. Then the Halim et al. found that $NH_4HF_2$ can be a substitute for HF to etch Al layers from the $Ti_3AlC_2$,[18] and Feng et al. concluded the following reactions:

$$Ti_3AlC_2 + XHF_2 \rightarrow X_aAlF_b + AlF_3 + H_2\uparrow + Ti_3C_2 \quad (4)$$

$$AlF_3 + cH_2O \rightarrow AlF_3 + cH_2O \quad (5)$$

$$Ti_3C_2 + XHF_2 + H_2O \rightarrow Ti_3C_2F_x(OH)_yX_z \quad (6)$$

where "X" represents the $K^+$, $Na^+$, $NH_4^+$, the a, b, c, x, y, and z are different numbers.[19] Etching with $NH_4HF_2$, however, will cause $NH_3$ or $NH^{4+}$ molecules to be inserted between MXene sheets. Followed by LiF/HCl etching method, which was used by Ghidiu et al. to etch $Ti_3AlC_2$ powers. The LiF can react with HCl to produce HF to etch MAX phase. This method can be versatile because the LiF/HCl solution can etch other MAX phases like $Nb_2AlC$ and $Ti_2AlC$. When the LiF is replaced with other fluoride salts, such as $CaF_2$, KF, CsF, and NaF, the etching behavior is similar, if $H_2SO_4$ takes the place of HCl, the MXene can also be obtained.[3] But this method will make MXenes possess a lot of oxygen-containing surface groups. In order to solve the problem that the Al layers can't be etched out from nitride-based in aqueous acidic solutions, Patrick Urbankowski et al. used molten fluoride salt for the purpose of etching Al from $Ti_4AlN_3$ powder at 550°C under argon atmosphere in 2016. And the resulting MXenes are predicted to be metallic and magnetic.[20] In late 2016, the MILD method, of which full name is minimally intensive layer delamination method, appears. The MXenes obtained by this method possess the best quality compared with those above methods. For example, Sang et al. take

advantage of this method to exfoliate MAX phase to synthesize free-standing monolayer $Ti_3C_2T_X$.[21] To overcomes the disadvantages of using highly toxic fluorine etching agent and long etching time in the conventional synthetic route which limits biomedical applications, Song et al. synthesized fluoride-free $Nb_2CT_x$ through electrochemical etching exfoliation. Then a biosensor for phosmet detection was constructed based on fluorine-free $Nb_2CT_X$ which showed superiority to the $Nb_2CT_X$ biosensor etched by hydrofluoric acid and the enzyme activity and electron transfer of the biosensor are enhanced by fluorine-free MXenes.[22] In addition to the classification determined by etching methods, these methods can also be classified by MAX phases such as Al-attaching MAX-phase precursor, Ga-attaching MAX-phase precursor, Si-attaching MAX-phase precursor, and non-MAX phases such as $YAl_3C_3$ and $Zr_3Al_3C_5$(where an $Al_3C_3$ unit instead of an Al atomic layer is etched out).[23–26]

With regard to the etching of MXene, physical methods such as ultraviolet (UV) irradiation can also be used for etching besides chemical methods. According to reports, ultraviolet irradiation can enhance the surface reaction of some semiconductors. For example, $Mo_2Ga_2C$ is a promising ultraviolet absorbing material and its absorption from infrared to ultraviolet region increases. Then Mei et al. reported a novel UV-assisted selective etching method to synthesis MXene in a much greener way. The fabrication process of 2D mesoporous $Mo_2C$ MXene is as follows: phosphoric acid was added into the precursor of $Mo_2Ga_2C$ and stirred under UV irradiation firstly, then the resulting product was washed with deionized water until pH was close to 7, following by ultrasonicated, and finally centrifuged and dried. In a word, the combination of ultraviolet irradiation and weak acid chemical etching can significantly promote the etching of Ga layer from $Mo_2Ga_2C$ precursor, avoid the use of dangerous acid and the termination of fluorine, as well as introducing the final mesoporous structure into MXene. The obtained MXene has a unique 2D graphene-like structure and high purity.[27]

## 2.2 | Bottom-up method

Compared with those commonly used top-down methods, these bottom-up methods are not commonly seen. Perhaps due to the complex element composition, structure inside MXenes and the mechanism of interaction between the components is still unclear. However, the bottom-up method has some advantages that the top-down method doesn't have such as controllable structure, composition, size, and morphology, which are significantly vital to the performance of the MXenes. Through crystal growth, methods for synthesizing MXenes from the atomic level include chemical vapor deposition (CVD), template method (Figure 2B) and plasma - enhanced pulsed-laser deposition (PE-PLD).[28] For instance, Xu et al. fabricated the 2D ultrathin $Mo_2C$ crystals with high quality and large area through CVD firstly in 2015.[29] The obtained crystals' thickness is a few nanometers, with a size of over 100 μm. Besides, this CVD process can be available for the fabrication of other MXenes, such as WC,[30] which further expands the family of MXenes and gives more choices of synthesis. Then, during the next few years, various composite compounds are synthesized through this method, such as $Mo_2C$/graphene heterostructures,[31] $Mo_2C$-graphene ($Mo_2C$ - Gr) hybrid film[32] and so on. In 2017, some researchers developed a new method based on CVD. Generally, this method is a two-step method, transition metal oxides are synthesized as template through CVD firstly, and then nitriding or carbonizing them. For example, Xiao et al. annealed Mo-precursor covering NaCl crystals to obtain 2D $MoO_3$ nanosheets, then the obtained 2D $MoO_3$ nanosheets were taken as templates to synthesize 2D h-MoN nanosheets.[33] After that, Joshi et al. synthesized 2D-layer $MoO_3$ using hot-filament chemical vapor deposition at first, then the obtained product was transformed to 2D-MoN under the ammonia atmosphere at 800°C.[34] In addition to the above two methods, plasma-enhanced pulsed-laser deposition(PE-PLD) is also a method to fabricate MXenes, which combines the advantages of both plasma–enhanced CVD (PECVD) and pulsed-laser deposition (PLD). For example, Zhang et al. successfully grew continuous single-crystalline $Mo_2C$ films with different thicknesses which are controllable by the laser pulse number on sapphire (0001) under 700°C.[35] Also, this method is suitable for the synthesis of other MXenes. Despite of these good points, there are still some problems such as synthesis of mono-layer and large-area MXene nanosheets, large-scale fabrication, visible defects in MXenes that need to be addressed.

In a word, Figure 2C shows the synthetic methods of MXenes that have appeared so far and their corresponding time of the first occurrence.

# 3 | STRUCTURES AND PROPERTIES

As emerging two-dimensional materials, MXenes show definite properties compared with other materials, such as excellent electronic properties, outstanding optical properties, extraordinary magnetic properties, superior hydrophilic as well as flexible mechanical properties. As we all know, structures are associated with properties, while properties lead to applications. Then the structures and properties will be introduced in the following sections.

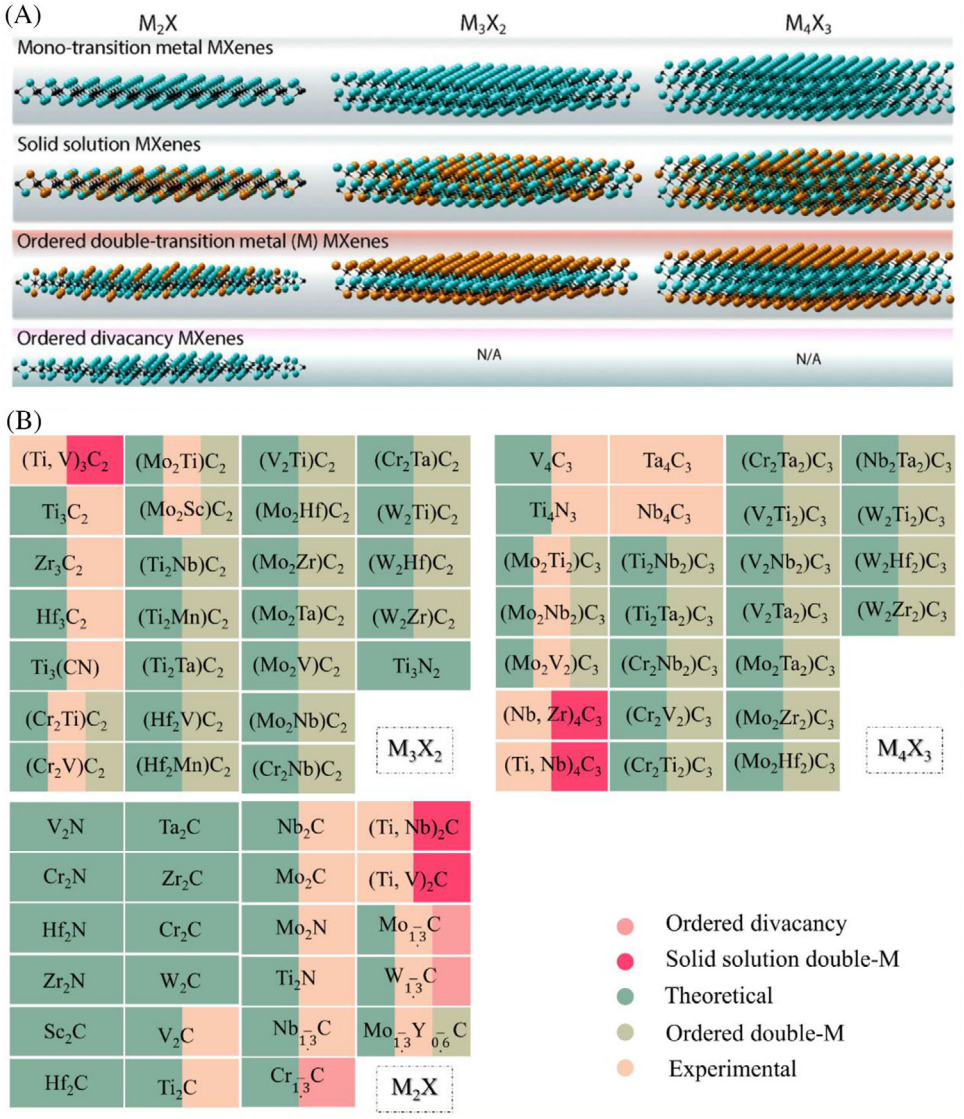


**FIGURE 3** A, According to the composition, MXenes can be divided into three different formulas: $M_2X$, $M_3X_2$, $M_4X_3$. On the basis of structure, MXenes can also be divided: mono-transition metal MXenes, solid solution MXenes, ordered double-transition metal(M) MXenes, ordered divacancy MXenes. Reproduced with permission.[36] Copyright 2019, American Chemical society. B, MXenes reported so far, including theoretical prediction and experimental synthesis

## 3.1 | Structures of MXenes

Up to date, the structures of MXenes can be divided into four types: mono-transition metal MXenes, such as $Ti_2C$ and $Nb_4C_3$; solid solution MXenes, such as $(Ti, V)_3C_2$ and $(Ti, V)_2C$; ordered double- transition metal (M) MXenes, such as $(Cr_2V)C_2$ and $(Mo_2Ti_2)C_3$; and ordered divacancy such as $Mo_{1.33}C$ and $W_{1.33}C$[36] (Figure 3A, B).

In addition to the common two-dimensional structure of MXenes (Figure 4A), there is one-dimensional structure (Figure 4B, C), three-dimensional structure (Figure 4D) and quasi-zero-dimensional structure (Figure 4E). Compared with the two-dimensional structure that has been studied a lot, MXenes of one-dimensional structure have fewer investigations. Zhao et al. constructed $Ti_{n+1}C_n$ (n = 1, 2) and $V_2C$ nanoribbons to study their properties and two types of armchair and six types of zigzag nanoribbon were considered. All of them possess unique properties, especially manageable magnetism, and some of them have larger band gaps compared with pristine MXenes nanosheets.[37] Apart from nanoribbon, Pang et al. report a HF-free method that is capable of synthesizing 1D $Nb_2CT_x$ nanowire with dilute HCl electrolyte in 4 hours[38] Although two-dimensional MXenes have many advantages, their aggregation and self-restacking are also problems that can be seen usually during the fabrication process. Then some researchers consider assembling 3D architectures with 2D MXene nanosheets to fix

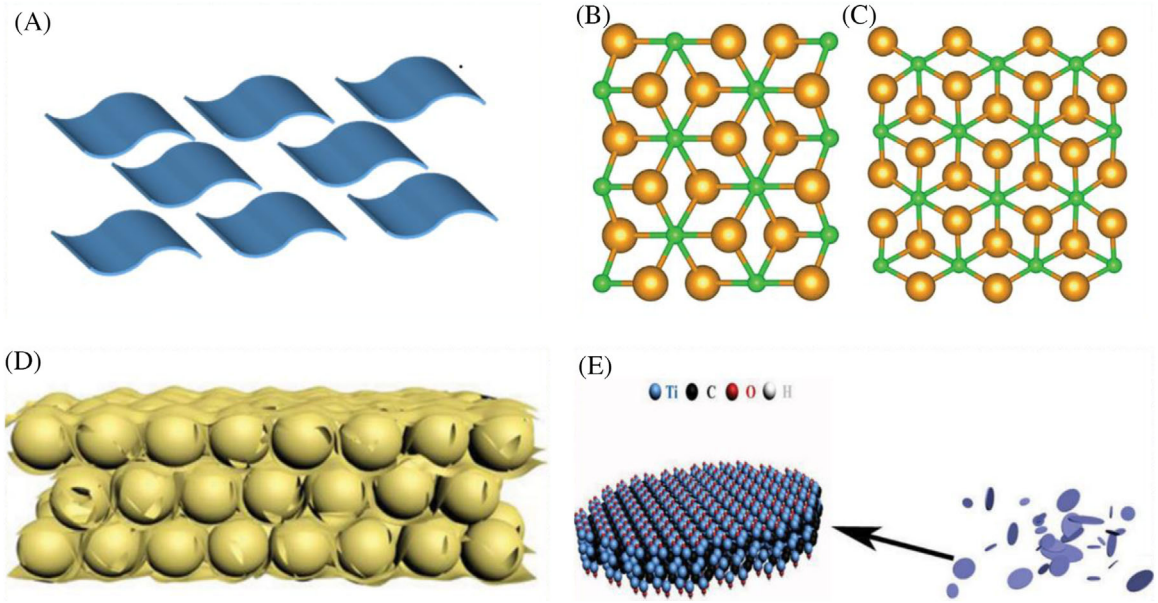


**FIGURE 4** The 1D, 2D, 3D, and 0D structures of MXenes. A, Two-dimensional structure of MXene nanosheets. Top view of the geometric structures of (B) zigzag and (C) armchair $Ti_2C$ nanoribbons. Yellow and green balls indicate Ti and C atoms, respectively. Reproduced with permission.[37] Copyright 2015, Royal Society of Chemistry. D, The 3D M-$Ti_3C_2T_x$ film. Reproduced with permission.[40] Copyright 2020, Wiley. E, The nonoxidized MXene-$Ti_3C_2T_x$ quantum dots (NMQDs-$Ti_3C_2T_x$) prepared by microexplosion method. Reproduced with permission.[47] Copyright 2020, Wiley

problems of restacking for the purpose of larger specific surface area, higher porosity, as well as shorter transport distance of ion and mass over normal 1D and 2D structures.[39] For example, Li et al. took PS (polystyrene) spheres as a template to fabricate $Ti_3C_2T_x$ electrodes with a 3D structure. The obtained freestanding and flexible 3D-macroporous $Ti_3C_2T_x$ (3D M-$Ti_3C_2T_x$) film has an open and interconnected structure. The electrical conductivity of the film was about 600 S $cm^{-1}$, which is higher than that of 3D graphene film with a similar structure (≈12 S $cm^{-1}$).[40] And, Shah et al. showed that the $Ti_3C_2T_x$ nanosheets have the ability to be scrolled, bent, and folded into 3D wrinkled structures after encapsulated with spray-dried droplets. After rehydration, the changes in morphology can be restored to the original state.[41] Besides, 2D MXene nanosheets can be assembled into 3D porous architectures with other materials such as reduced graphene oxide (rGO),[42] melamine,[43] SnS[44] and so on. These MXenes with 3D structure mostly used for energy storage, such as supercapacitors, lithium-ion batteries, sodium-ion batteries, lithium-sulfur batteries and electrocatalysis. In addition to the above 1D, 2D, 3D structures, there are 2D MXenes-derived QDs (MQDs). Even though in an early stage, they have many advantages such as high electrical conductivity, plentiful active sites, remarkable dispersibility, tunable structure, great hydrophilicity, excellent optical properties, multiple functionalization, and so on.[45] Thus, they can be used in the fields of sensing, catalysis, energy storage, biomedical science and optoelectronic devices. For example, Guo et al. using hydrothermal treatment to prepare $Ti_3C_2$ QDs from $Ti_3C_2$ MXenes. When in an aqueous solution, the obtained $Ti_3C_2$ QDs showed excellent tolerance to salt, anti-photobleaching and dispersion stability. Moreover, they can determine alkaline phosphatase (ALP) activity with a low limit of detection (0.02 U $L^{-1}$) and monitor the enzyme activity in real-time to identify embryonic stem cells (ESC).[46] Though so many great achievements, there are still some challenges that need to be noted, such as synthesis methods, properties, functionalized modification, biocompatibility and cytotoxicity of MQDs. Besides, more effort should be devoted to exploring more applications.

## 3.2 | Electrical properties

Compared with other properties, electronic properties have been studied mostly. Interestingly, all bare MXenes monolayers are metallic, while OH, F, O terminations can cause the metal-semiconductors transition. There are some factors that affect the electrical performance of MXenes, such as the preparation process, surface termination, elemental composition, inner structures and surrounding conditions like humidity, pH,

temperature and so on. Thus, the electronic properties can be adjusted by the following means: (i) changing the "M" elements, which are mostly related to metallic of MXenes; (ii) improving synthesis methods that making fewer defects, such as the use of fluorine-free synthesis; (iii) changing the surface groups to tune bandgaps, for example, removing OH-contained groups or adding O-contained groups; (iv) increasing the interlayer distance which contributes to the energy density; (v) designing new structures. For example, Ran et al. prepared the MXene film electrode through the freeze-drying technique to alleviate its self-restacking and improve the electrochemical performances. Through freeze-drying treatment, the frozen solvent molecules were removed by sublimation, and alleviated the adverse effect of van der Waals forces and enlarging layer space. The obtained freeze-dried MXene (f-MXene) films show unique porous architecture with highly efficient ion diffusion and transport channels.[48] Benefit from their outstanding electronic properties, MXenes are mostly used in energy store, besides, they can be applicable for biomedical fields. For example, when specific biomolecules are attached to the surface of MXenes, the electrical conductivity of MXenes will be changed to achieve the purpose of biomolecule detection. Also, the electronic properties make them suitable for the manufacture of wearable electronic devices to monitor the body's physiological signals.

## 3.3 | Optical properties

For applications of MXenes, optical properties are also important which include absorption, transmission, photoluminescence, saturation absorption, nonlinear refractive index, scattering, emission, and so on. These properties are highly dependent on their energy structure such as energy band gap, direct/indirect band gap, topological properties, etc,[49] while the energy band structure of MXenes is mainly affected by surface groups, external electric field, stress, doping, and electronic localization. Noting that, compared with 2D MXenes nanosheets, MQDs have stronger photoluminescence (PL) emission. Because of these properties, MXenes can be applied in many fields like photocatalysis, sensing and biomedical such as photoacoustic imaging, photothermal therapy (PTT), photodynamic treatment (PDT), controlled drug release and biosensing. Since MXenes show strong light absorption in the near infrared region (NIR) with the ability of high photothermal conversion owing to localized surface plasmon resonances, they are often used to ablate tumors in biomedical applications. Because these $Ti_3C_2$ MXenes possess not only a high drug loading capacity of 211.8%, but also the characteristics of pH sensitivity and near-infrared laser on-demand trigger drug release, the cooperative treatment of chemotherapy and PTT is achieved. Also, these $Ti_3C_2$ MXenes have also proved to be ideal photoacoustic imaging contrast agents, demonstrating the potential for diagnosis, imaging guidance and monitoring during treatment. Thus, MXenes can get the purpose of monitoring the lesion while achieving synergetic treatment.[50] It is worth mentioning that the optical characteristics can also be adjusted by altering thickness,[51] intercalation, such as ion intercalation[52] and molecule intercalation (TMAOH, or $NMe_4OH$),[53] changing M, which is related to the visible light absorption range,[54] tuning their surface terminations to adjust the band gaps to fit the UV light, for example, the O-terminated $Ti_3C_2T_x$ offering the best catalytic activity.[45,55]

## 3.4 | Magnetic properties

Compared with the electronic and optical properties, the magnetic properties of MXenes are less studied. When the Stoner criterion $I \cdot N(E_f) > 1$, the high values of $N(E_f)$ can result in a magnetic instability, making MXenes magnetic.[56]It is worth noting that $Ti_2CO_2$, $Zr_2CO_2$, $Hf_2CO_2$, $Sc_2CO_2$, $Sc_2C(OH)_2$, $Cr_2C(OH)_2$, $Cr_2CF_2$, and $Sc_2CF_2$ are considered to be semiconductors and nonmagnetic among MXenes.[57] The magnetic properties of MXenes include ferromagnetic(such as $Cr_2C$[58])and antiferromagnetic (such as $Ti_3C_2$, $Cr_2TiC_2F_2$[59]).[60] Similar to the optical and electrical properties, the magnetic properties of MXenes are also affected by many factors such as the composition of "M" and surface termination. For example, Zhong et al. proposed $V_2N$ with the structure of Janus in which one V layer is replaced with Ti/Cr layer. Making use of the first-principles calculations, they showed that although the antiferromagnetic (AFM) ground states are formed, the TiVN and CrVN monolayers possess net magnetic moments of 1.97 and 0.28 mu(B) per formula unit, respectively. In addition, when a considerable strain (-8% to 8%) is applied to the TiVN and CrVN monolayers, their net magnetic moments are also very stable.[61] Moreover, surface groups are also vital to the magnetic properties of MXenes. The presence of surface terminals causes the magnetism of MXenes to disappear because of the p–d bonds between the M atoms and T groups, which results in a partial depopulation of the near Fermi states, then the value of $N(E_f)$ reduces, except for $Cr_2C$ and $Cr_2N$.[56] Besides, external conditions can also affect the magnetic properties of MXenes. For example, Lv et al. have found that monolayer $Ti_2C$ changes from an AFM semiconductor to a ferrimagnetic (FIM)

semiconductor, half-metal, magnetic metal, non-magnetic (NM) metal, and NM semiconductor when applying an external electric field. Besides, while the electric field increases beyond a certain value, the magnetic moments of Ti atoms decrease drastically, at this time, the effective masses decrease remarkably, while the conductivity increases. Thus, the magnetic properties can be adjusted through the external electric field.[62] Importantly, MXenes can also be a promising electromagnetic interference (EMI) shielding material, which is more than 70 dB at merely 0.8 mm in X-band. Not only does the multilayered structure strengthen the internal electromagnetic (EM) attenuation, it also enhances the absorption efficiency apparently. Furthermore, the high electrical conductivity makes the EM reflection on the surface sufficient.[63] Although MXenes, by virtue of their magnetic properties, have been outstanding contrast agents for bioimaging. The EMI shielding performance of MXenes for biomedical research needs to be developed.

### 3.5 | Hydrophilicity and biocompatibility

Surfaces hydrophilic nature of MXenes was given by the surface terminations including hydroxyl (-OH), oxygen (-O), or fluorine(-F). The contact angle measurements using deionized water on the surface of the cold-pressed MXenes disc found that MXenes have hydrophilicity and good electrical conductivity.[17] Thus, the hydrophilic properties of MXenes with high conductivity makes them interact with the polymer matrix better, which is beneficial to their use in composite materials.[64] Besides, hydrophilicity is usually related to biocompatibility. Generally speaking, better biocompatibility makes hydrophilicity higher. Although there are not many studies on the biocompatibility of MXenes, some common Ti-based MXenes are found to be biocompatible such as $Ti_3AlC_2$.[65] Therefore, MXenes, which combine conductivity, hydrophilicity and 2D layered atomic structures, can be promising candidates to manufacture biologically compatible field-effect transistors (FET) to investigate biological events in a speedy, direct, and label-free way.[66] Noting that their hydrophilic behavior is also beneficial to the surface functionalization and antibacterial activity of MXenes which may facilitate the inactivation of bacteria through direct contact interactions.[67] In addition, hydrophilicity and large surface area of MXenes make them possess the capacity of drug-loading. As we all know, the hydrophilic property will promote adsorption for polar or ionic molecular. Therefore, another potential application of MXenes is in the environment to adsorb harmful substances.

### 3.6 | Mechanical properties

In addition to the above properties, the mechanical properties of MXenes have aroused great interest, too. The atomic layer thickness of MXenes gives MXenes mechanical flexibility, while MXenes' mechanical properties depend on their surface terminations (the O-terminated MXenes have very high stiffness, which may be related to the larger lattice parameters) significantly. What's more, the mechanical properties are tested by strain tests, and the resulting elastic constants are used to evaluate the mechanical properties of MXenes. Materials with good mechanical properties can be used in many fields of strain sensors, energy storage, wearable electronics, etc. Thus, it is important to understand the mechanical nature of MXenes under deformation fully. Guo et al. took 2D $Ti_{n+1}C_n$ (n = 1, 2 and 3) as examples to study the tensile stress-strain curves of MXenes which were under different loading directions through first-principles calculations systematically. The calculated results showed that 2D $Ti_2CO_2$ can sustain larger strains compared with graphene because of the surface functionalizing oxygen. What's more, the collapse of the Ti layer will be retarded by the surface functionalization, and the critical strain of 2D $Ti_2C$ increased apparently. Moreover, the critical strains did not change much but Young's modulus decreased slightly with n in $Ti_{n+1}C_n$ increasing from 1 to 3. In a word, the surface functionalization can reduce Young's modulus, extend the critical strains to improve their mechanical properties and enhance mechanical flexibility.[68] And the number of atomic layers is also a factor affecting mechanical properties. Apart from these, the mechanical properties will also be improved after forming a composite material with other materials. For example, Cao et al. combined 2D MXenes with a scale of micro-nano and 1D cellulose nanofibers with strong hydrogen bonds through mesoscopic assembly to obtain a soft actuator with layered gradient structure. The actuator has the advantages of the high tensile strength (237.1 MPa), high Young's modulus (8.5 GPa), and excellent toughness (10.9 MJ $m^{-3}$) with direct and rapid moisture absorption in a single body.[69] Some flexible wearable sensors can be designed based on the mechanical properties of MXenes. Physical activity deforms these sensors and sends out electrical signals to detect human activity and physiological signal in real time.

## 4 | SURFACE MODIFICATION AND ENGINEERING OF MXENES

Although MXenes possess outstanding electronic properties, excellent optical properties, fascinating magnetic

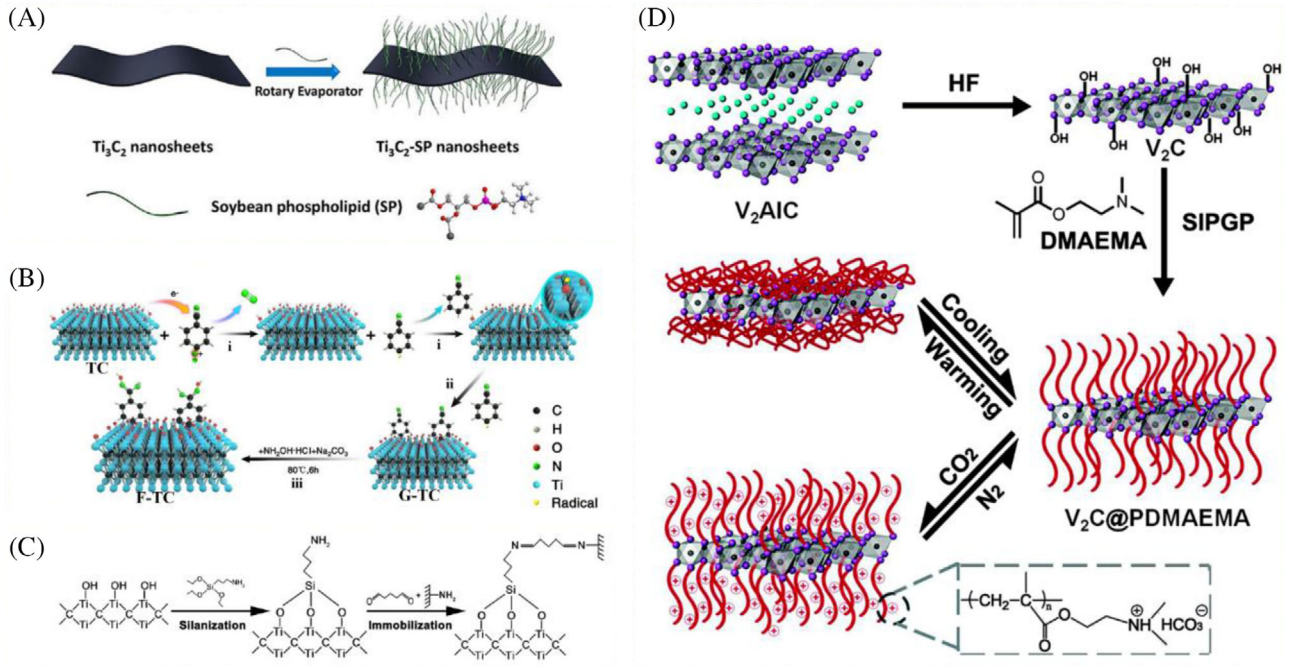


**FIGURE 5** Polymer-based strategy of surface chemistry. A, Schematics of $Ti_3C_2$ nanosheets modified with SP. Reproduced with permission.[12] Copyright 2017, American Chemical Society. B, Mechanism for functionalization of $Ti_3C_2T_x$ MXene. Reproduced with permission.[72] Copyright 2020, American Chemical Society. C, Schematic illustration of lipase immobilization through covalent bonding. Reproduced with permission.[74] Copyright 2019, Elsevier. D, Progress of making $V_2C$@PDMAEMA smart hybrid system. The C atoms are represented by gray, V atoms by purple, and Al atoms by blue. For simplicity, only two layers of $V_2C$ are shown here. Reproduced with permission.[75] Copyright 2015, Royal Society of Chemistry

properties, hydrophilic, and biocompatibility as well as tremendous mechanical properties, the bare MXenes are not stable and easily aggregate in physiological environments, thus, surface modification is required to optimize properties and promote wider application while not destroy the original 2D morphology. Since there are functional groups, charges of high density and a large area on the surface of synthetic MXenes, they can be modified by electrostatic adsorption, hydrogen bonding, van der Waals force, etc. In the next chapter, we will discuss three surface modification methods: compound-based strategy of surface chemistry, inorganic nanoparticle-based surface chemistry, and metal nanoparticle-based method of surface chemistry.[70]

## 4.1 | Polymer-based strategy of surface chemistry

Polymer-based surface modification strategies are mainly related to the engineering of certain molecules or polymers, such as polyethylene glycol (PEG), soybean phospholipid (SP), hyaluronic acid (HA), polyvinyl pyrrolidone (PVP), etc. In addition, their mixture can also modify the surface of MXenes. Polymers can be assembled to the surface of MXenes through the following methods: self-initiated photo-grafting and photopolymerization (SIPGP), aryl diazonium chemistry, non-covalent, physical adsorption interactions and so on. Non-covalent bonds and simple physical adsorption interactions are common surface modification strategies, which are used in the modification strategies of drug loading mostly.

For example, Lin et al. modify $Ti_3C_2$ nanosheets with SP, the obtained $Ti_3C_2$-SP nanosheets (Figure 5A) don't show any toxicities in both vitro and vivo. The intravenously injected MXenes will arrive and accumulate at the tumor area through the enhanced permeability and retention (EPR) effect.[12] However, most of the MXenes complexes synthesized by this method are unstable and the release of drugs can't be controlled, so they will be limited in the practical biomedical applications. Therefore, it is urgent to develop other new methods to modify surfaces for wider biomedical applications of MXenes and MXenes-based materials.[71] For example, aryl diazonium chemistry is a method to modify the surface of MXenes for the reason that the covalent bonds on the surface of all kinds of substrates can be formed by aryl diazonium. Zhang et al. placed the amidoxime chelating groups on $Ti_3C_2T_x$ MXenes surface through diazonium salt grafting successfully. The selectivity of $Ti_3C_2T_x$

nanosheets for uranyl ions and stability in aqueous solution are apparently improved because of the introduction of amidoxime functional groups. Thus, the uranium can be extracted from aqueous solutions containing competitive metal ions in an efficient, fast, and recyclable way (Figure 5B).[72] Apart from above, Liang et al. triggered the Fenton-based nano-catalytic reaction on 2D titania carbide ($Ti_2C_2$) MXenes nanosheets.[73] The specific synthesis process is as follows: firstly, the ferric sulfite was used as ferrous source, iron oxide nanoparticles (IONPs) were grown in situ onto the surface of 2D $Ti_3C_2$ MXene through surface redox reaction under the alkaline condition; then, taking advantages of amino-[poly (ethylene glycol)] ($NH_2$-PEG) to modify the surface of $Ti_3C_2$-IONP nanocomposites for the enhanced stability under physiological condition; at last, fixing glucose oxidase (GOD) making use of amidation interaction between modified 2D $Ti_3C_2$ MXene and GOD molecules. This approach makes MXenes more stable in the physiological environment and promotes the application of MXenes in biomedicine. In addition, Ding et al. modified $Ti_3C_2T_X$ nanosheets with (3-aminopropyl) triethoxysilane (APTS) to generate amine functional groups on the surface of $Ti_3C_2T_X$, firstly. Then, the obtained modified-$Ti_3C_2T_X$ nanosheets were treated with glutaraldehyde, and covalently coupled with lipase. It was found that the photothermal properties of $Ti_3C_2T_X$ nanosheets may cause a local temperature increase around the lipase when the hydrolysis reaction is carried out under the irradiation of near-infrared laser, resulting in enhanced enzyme activity of the immobilized lipase (Figure 5C). The functionalized $Ti_3C_2T_X$ nanosheets with lipase immobilized have outstanding pH sensitivity, thermal stability and reusability.[74] SIPGP is a facile polymerization method, which no more requires anchoring layers, self-assembled monolayers (SAMs) and initiators, while the only thing needed to do is grafting brush on the surface of materials in a one-step reaction at room temperature under UV-irradiation directly. Based on this, Chen et al. developed a robust strategy to graft poly(2-(dimethylamino) ethyl methacrylate) (PDMAEMA) on 2D $V_2C$ through SIPGP and investigated their $CO_2$ and temperature dual-responsive properties further in 2015 (Figure 5D).[75]

## 4.2 | Inorganic nanoparticle-based surface chemistry

In addition to the polymers, inorganic nanoparticles can also be used for surface modification. A classic drug delivery system (DDS), which integrates $Ti_3C_2$ MXene with mesoporous silica nanoparticles (MSN), is a typical example. Yang et al. developed a kind of surface nanopore engineering of 2D $Ti_3C_2$ MXene on the basis of a facile sol-gel chemistry for the first time. Cetane trimethylammonium chloride (CTAC) was employed as a mesopore-directing agent and tetraethyl orthosilicate (TEOS) as a silica precursor when in alkaline condition. This surface nanopore engineering integrates several unique properties such as definite mesopores with confined spaces for drug delivery, improved hydrophilicity/dispersity, and plentiful surface chemistry for surface engineering (Figure 6A).[76] Also, MXenes and nanoparticles can be integrated into biosensors. Wang et al. synthesized an organ-like $Ti_3C_2$ MXene ($TiO_2$-$Ti_3C_2$) nanocomposite modified with $TiO_2$ nanoparticle to immobilize hemoglobin (Hb) for the purpose of mediator-free biosensor fabrication (Figure 6B). The obtained $TiO_2$-$Ti_3C_2$ nanocomposite is an outstanding immobilization matrix with biocompatibility for redox protein and makes them possess excellent bioactivity and stability. The prepared biosensor can detect $H_2O_2$ in a very low detection limit of 14 nM with a linear range of 0.1–380μM (sensitivity 447.3 μA $mM^{-1}$ $cm^{-2}$).[77] Besides the common nanoparticles mentioned above, some inorganic nanoparticles are also used to modify the surface of MXenes such as ZnO,[78] $SnO_2$,[79] SnS,[80] CoS,[81] $NiFe_2O_4$,[82] $Mn_3O_4$,[83] etc.

## 4.3 | Metal nanoparticle-based method of surface chemistry

Despite the common surface modifications with compounds and inorganic nanoparticles, the modification with noble metals can improve the properties of MXenes effectively and make applications of MXenes wider. In which, the modifications with gold, silver and platinum are common. The 5 nm gold nanoparticles (AuNPs) casted on double screen-printed gold electrodes are used to modify MXene-$Ti_3C_2T_x$ by Mohammadniaei et al. to contain a large number of DNA probes co-immobilized on a special electrode. Not only can the presence of MXenes provide biofouling resistance, they also increase the electrochemical signal by nearly four times. The 5 nm AuNPs are well distributed in the entire flake structure of MXenes, thereby enhancing the electrochemical performance of MXene and providing the characteristics of the thiol-Au bond. The proposed collaborative strategy reduces the analysis time of duplex-specific nuclease (DSN)-based biosensors to 80 minutes with antifouling activity, significant sensitivity and specificity (single mutation identification).[84] In order to solve the problem of low flux and fouling during membrane separation, Ravi P. et al. reported 2D MXenes ($Ti_3C_2T_x$) modified with Ag nanoparticles (Ag@MXene) for the use of ultrafast water purification. The composite membrane with tunable AgNPs loadings (between 0% and 35%) was fabricated through the self-reduction of silver

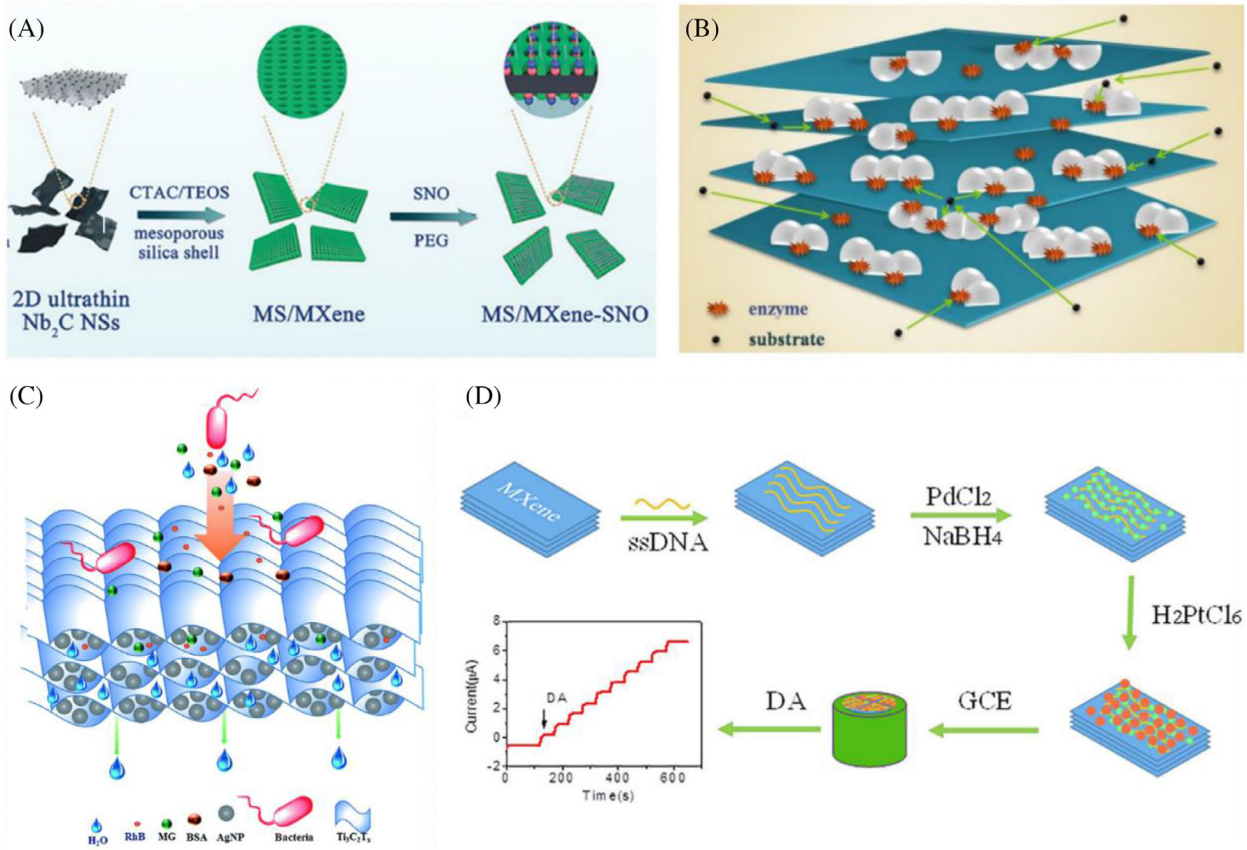


**FIGURE 6** Inorganic nanoparticle-based and metal nanoparticle-based surface chemistry. A, Fabrication of MBS (multifunctional therapeutic platform). Reproduced with permission.[76] Copyright 2020, Wiley. B, The organ-like structure of $TiO_2$–$Ti_3C_2$ nanocomposite encapsulating hemoglobin. Reproduced with permission.[77] Copyright 2015, Elsevier. C, Schematic diagram of 21% Ag@MXene composite membrane structure and rejection mechanism. Reproduced with permission.[85] Copyright 2018, Royal Society of Chemistry. D, Schematic diagram of $Ti_3C_2$/DNA/Pd/Pt nanocomposite synthesis. Reproduced with permission.[86] Copyright 2018, Elsevier

nitrate on the surface of MXenes in solution, in which the MXenes can form membranes and act as reducing agents. The 21% Ag@MXene membrane with a thickness of 470 nm and an average pore size of 2.1 nm has a higher flux (~ 420 $Lm^{-2}$ $h^{-1}$ $bar^{-1}$) compared with the original MXenes (~118 $Lm^{-2}$ $h^{-1}$ $bar^{-1}$) under the same conditions. In addition, the 21% Ag@MXene membrane has high rejection efficiency of organic molecules and an excellent flux recovery rate. What's more, more than 99% of E. coli growth is inhibited, while the unmodified MXenes membrane only showed close to 60% inhibition of bacterial growth. Compared with other membranes that have been reported, 21% Ag@MXene membrane has good repellency against organic dirt such as bovine serum albumin (BSA) and methyl green (MG) (Figure 6C).[85] In most cases, platinum will modify MXenes together with other nanoparticles. For instance, Zheng et al. fabricated a novel MXene-based nanocomposite (MXene/DNA/Pd/Pt) to develop sensitive dopamine (DA) sensors. In which the MXenes nanosheets acted as the conductive matrix for Pd/Pt nanoparticle loading. Due to the presence of aromatic hydrophobic groups, DNA will be adsorbed on the surface of MXenes, not only does it make $Ti_3C_2$ nanosheets disperse well, it also contributes to the uniform growth of Pd NPs and Pd/Pt nanoparticles. And the Pd/Pt nanoparticles obviously gave rise to the electrocatalytic activity of nanocomposites on DA (Figure 6D).[86] In addition, Co[87] and Bi[88] nanoparticles can be used to modify the surface of MXenes to improve the photoelectric catalytic performance and charge transfer performance as well as sensing performance respectively.

## 5 | BIOMEDICAL APPLICATIONS

MXenes can be used in many biomedical applications of sensors, bioimaging, tissue engineering, photothermal therapy, antibacterial, drug delivery system, and so on due to their unique 2D layered structure and excellent physical and chemical properties including hydrophilicity, biocompatibility, light-to-heat conversion performance, and mechanical flexibility, etc. Next, we will introduce

the applications of MXenes in biomedical applications in detail.

## 5.1 | Sensors in biomedical applications

### 5.1.1 | Biosensors

Biosensing is used to selectively detect specific substances in the human body and mainly consists of the following parts: (i) a sensing element like an immobilized biomolecule that identifies its complementary analyte; (ii) a transducer, that has the ability to transform the biochemical signal to electrical signal and other signals such as optical signal and (iii) a data interpretation unit.[89] MXenes have become an emerging material for making biosensors due to their large surface areas, 2D layered atomic structures, excellent electrical properties, outstanding hydrophilicity, extraordinary optical properties, and abundant surface functional groups.

*Biosensing based on electrical signals*

Electrical signals-based biosensor refers to the sensor of which electrical properties on the surface changes by combining with analytes that are usually proteins, amino acids, RNA, $H_2O_2$, and so on, which is used for early diagnosis of diseases. Among analytes, glucose and $H_2O_2$ are relatively common. $H_2O_2$ is active oxygen and by-products of some oxidases in the body as well as the main medium for phagocytic cells. However, excessive active oxygen generated under pathological conditions will damage the cell membrane, protein, amino acids, etc. in the organism, so the effective detection of $H_2O_2$ for a certain early diagnosis of these diseases is very important. Direct electron transfer (DET) between enzyme and electrode is vital for making mediator-free electrochemical sensors. However, the enzymes are easily inactivated most of the time and the redox center of the protein is deeply embedded in the protein shell, which makes DET difficult. Thus, Wang et al. prepared a new kind of MXene-$Ti_3C_2$ nanomaterial with an organ-like structure successfully through HF etching at room temperature. The obtained MXene-$Ti_3C_2$ with excellent enzyme immobilization ability and biocompatibility was employed to immobilize hemoglobin (Hb) to manufacture a mediator-free biosensor and showed good biological activity and stability to protein. A possible reaction mechanism of $H_2O_2$ catalyzed by the Hb-based electrode is described as follows:

$$\mathrm{Hb}\left(\mathrm{Fe^{III}}\right) + \mathrm{e^-} \rightarrow \mathrm{Hb}\left(\mathrm{Fe^{II}}\right) \quad (7)$$

$$\mathrm{Hb}\left(\mathrm{Fe^{II}}\right) + \mathrm{H_2O_2} + 2\mathrm{H^+} \rightarrow \mathrm{Hb}\left(\mathrm{Fe^{III}}\right) + 2\mathrm{H_2O} \quad (8)$$

Because of the unusual structures and characteristics of MXene-$Ti_3C_2$ nanomaterials, the DET of Hb was promoted, and the prepared biosensor showed good detection performance of $H_2O_2$ with 0.1–260 μM of linear range and 20 nM of the detection limit.[90] In addition, the MXene-Au @Pt nanoflower composites possessing good conductivity and biocompatibility are fabricated by Wang et al. through one-step synthesis. Based on the above composites, MXene-Au @Pt/5′-nucleotidase/xanthine oxidase/bovine serum albumin (BSA) double-enzyme biosensor is fabricated, and the qualitative and quantitative detection of inosine monophosphate (IMP) is achieved by the by-product $H_2O_2$ produced after enzymatic hydrolysis.[91]

Apart from detecting $H_2O_2$, MXenes-based biosensors can also be used for the early diagnosis of cancer, such as nucleic acid,[84,92,93] amino acid,[94] protein.[95–97] Mohsen et al. proposed a synergetic amplification strategy that combines an electrochemical signal amplification based on AuNP-decorated MXene-$Ti_3C_2T_x$ and a duplex-specific nuclease (DSN)-based amplification system to detect multiple microRNAs in total plasma. The obtained biosensor possesses the following advantages: short assay time of 80 minutes; the multiplex ability of antifouling property, sensitivity and specificity (single mutation recognition); the limit of detection for microRNA-21 and microRNA-141 was measured 204 and 138 aM respectively with a broad linear range from 500 to 50 nM (Figure 7A, B).[84]

Due to the advantages of apparent affinity, substantial sensitivity, the simple process of synthesis and high-temperature stability for aptasensors, many researchers have explored the wider application of aptamer chains in disease diagnosis. For example, Zhou et al. made an electrochemical aptasensor on the basis of nanostructured multicomponent hybrid of $Ti_3C_2T_x$ nanosheets and $PMo_{12}$ nanoparticles, and the obtained aptasensor was embedded in polypyrrole (PPy) matrix for integration to detect the cancer marker, osteopontin (OPN) sensitively. This PPy@$Ti_3C_2T_x$/$PMo_{12}$-based aptasensor demonstrated apparent sensitivity for OPN, with a LOD of 0.98 fg $mL^{-1}$ and a broad linear concentration range from 0.05 to 10.0 ng $mL^{-1}$. What's more, the obtained aptasensor possessed excellent sensing properties with outstanding selectivity, good stability, appropriate regenerability, and applicability in human serum samples.[97]

In addition, electrical signals-based biosensors can also be used to detect nitrite,[98] glucose,[99–103] organophosphate pesticides,[104–107] glutathione,[108] epinephrine,[109] l-cysteine,[110] dopamine,[111] and action potentials in primary neurons,[66] etc.

*Biosensing based on optical signals*

Optical signals-based biosensors are mainly divided into electrochemiluminescence (ECL) biosensor and surface

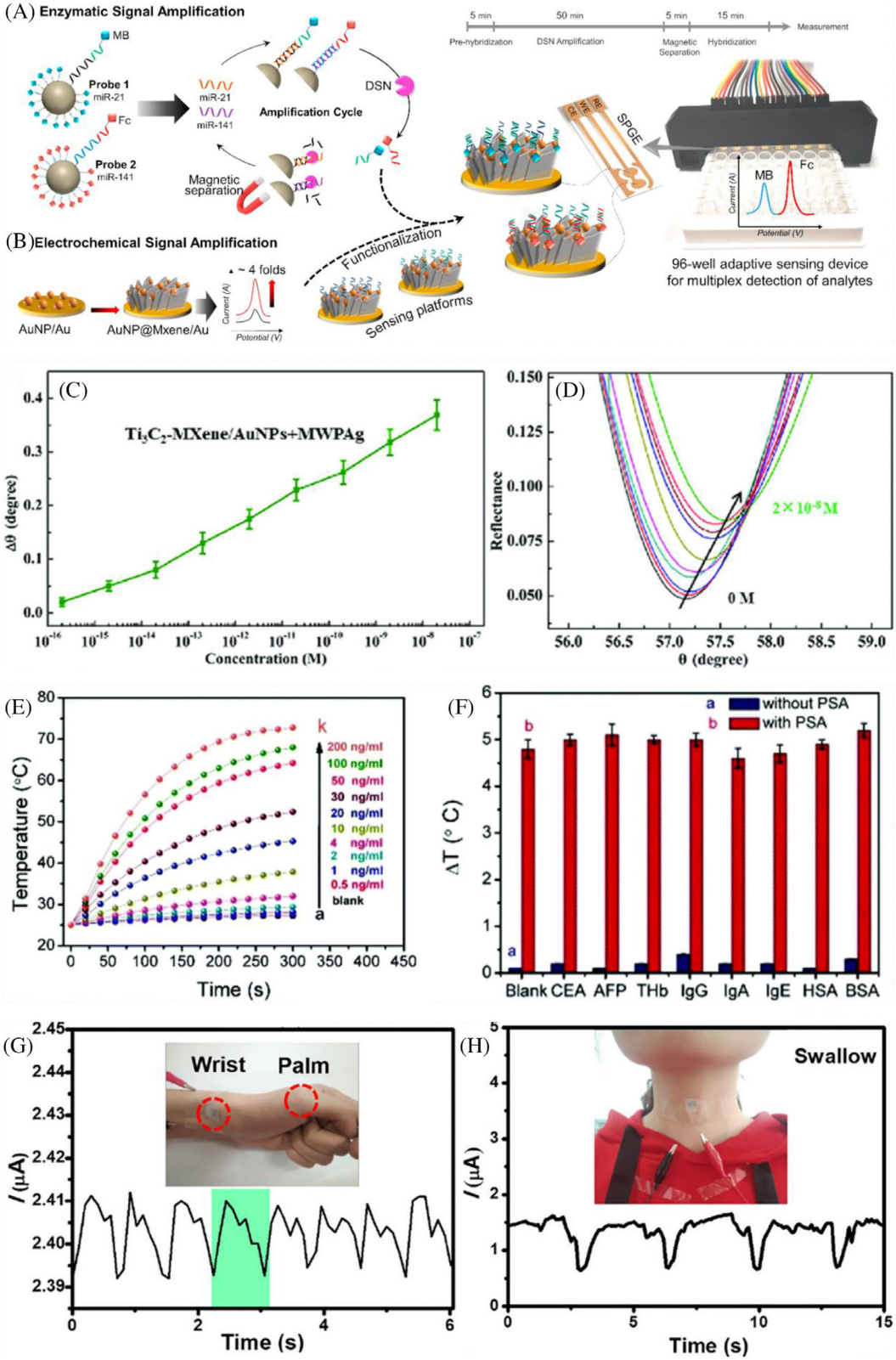


**FIGURE 7** MXenes for sensors in biomedical applications. (A-B) Schematic diagram of multiple and simultaneous detection of miR-21 and miR-141. Reproduced with permission.[84] Copyright 2020, Elsevier. (C-D) The relationship between CEA concentrations and SPR signal changes which are acquired by biosensor on the basis of $Ti_3C_2$-MXene/AuNPs sensing platform and MWPAg-$Ab_2$ signal enhancer. Reproduced with permission.[113] Copyright 2019, Elsevier. (E-F) The left picture shows the temperature responses (vs. time, under 808 nm irradiation) of the photothermal immunoassay, while the right picture demonstrates the selectivity of the photothermal immunoassay. Reproduced with permission.[115] Copyright 2019, Royal Society of Chemistry. (G-H) Sensing the wrist pulse and swallowing. Reproduced with permission.[119] Copyright 2019, American Chemical Society

plasmon resonance (SPR) biosensor according to the principle of illumination.

Due to its low background signal, high sensitivity, strong controllability, rapidness and low cost, ECL biosensor has been used in detecting proteins, DNA, enzymes and clinical diagnosis in the biochemical field widely. Zhang et al. utilized the aptamer recognition and catalytic ECL signal amplification of $Ti_3C_2$ MXenes nanosheets to fabricate a novel ECL biosensor. The efficient capture of exosomes on the electrode leads to a significant ECL signal response. The obtained MCF-7 exosome ECL biosensor showed high sensitivity, and its detection limit was 125 particles $\mu L^{-1}$, which was 100 times lower than the traditional enzyme-linked immunosorbent assay (ELISA) method. Besides, this ECL biosensor is flexible because it can be used to detect various exosomes in serum samples.[112]

Recently, SPR biosensors have become an important research tool in the fields of life sciences and pharmaceuticals with the advantages of followings: real-time detection, which can dynamically monitor the entire process of biomolecular interactions; free label samples, maintaining molecular activity; requirement of very few samples, generally only 1 mg of protein on a surface; convenient and fast detection process, as well as high sensitivity; wide application range; high-throughput, high-quality analytical data; ability to track and monitor the stability of fixed ligands. Then Wu et al. proposed an ultrasensitive SPR biosensor for the purpose of detecting carcinoembryonic antigen (CEA) which was comprised of a $Ti_3C_2$-MXene-based sensing platform and multi-walled carbon nanotube (MWCNTs)-polydopamine (PDA)-Ag nanoparticle (AgNPs) signal enhancer. Followed by the decoration with staphylococcal protein A (SPA) to align and fix the monoclonal anti-CEA antibody ($Ab_1$) through its Fc region. Then combining MWCNTs-PDA-AgNPs-polyclonal anti-CEA antibody (MWPAg-$Ab_2$) conjugate with a sandwich form to offer a dynamic range of $2 \times 10^{-16}$ to $2 \times 10^{-8}$ M for CEA determination with a limit of detection for 0.07 fM. The biosensing method showed apparent reproducibility with high specificity for CEA in real serum samples and can be used to assess CEA in human serum for the purpose of early diagnosis and monitoring of cancer (Figure 7C, D).[113]

In addition to the above two methods, chemiluminescence, and near-infrared (NIR) photothermal immunoassay can be used to detect target analytes. For instance, Li et al. synthesized a novel 2D MXene-$Ti_3C_2$/CuS nanocomposites with peroxidase-like activity through a facile hydrothermal method. Compared with the separate MXene-$Ti_3C_2$ nanosheet or CuS nanoparticle, the MXene-$Ti_3C_2$/CuS nanocomposites improved peroxidase-like activity synergistically and catalyzed the reaction of 3,3,5,5-tetramethylbenzidine (TMB) when $H_2O_2$ existed, which caused the blue color change. Then a facile colorimetric approach was used to detect $H_2O_2$ and cholesterol in the blood. The detection limit and linear range of $H_2O_2$ are 3.1μM and 0.1 –1 nM respectively, and the detection limit and the linear range of cholesterol are 1.9and 10–100μM respectively.[114] And Cai et al. made use of $Ti_3C_2$ QDs-encapsulated liposomes with outstanding photothermal efficiency to devise a NIR photothermal immunoassay for the qualitative or quantitative detection of prostate-specific antigen (PSA).[115] In addition to being an innovative photothermal signal beacon, $Ti_3C_2$ QDs are encapsulated in liposomes to label secondary antibodies. Besides, $Ti_3C_2$ QDs can convert light energy to heat energy when receiving NIR laser irradiation. Under the best conditions, the $Ti_3C_2$ QD-based photothermal immunoassay showed a dynamic linear range for PSA from 1.0 to 50 ng $mL^{-1}$ and the LOD was 0.4 ng $mL^{-1}$. What's more, a portable device constructed with NIR imaging cameras was used to collect visual thermal data to perform semi-quantitative analysis of the target PSA within 3 minutes (Figure 7E, F).[115]

### 5.1.2 | Physical sensors

In addition to some biomolecules which can change the electrical signal of MXene-based sensors, the pressure and tension also make electrical signal of the sensors change due to the excellent electronic properties and mechanical properties of MXenes. Thus, the sensors can also be designed for flexible wearing to detect human activity and physiological signal in real time.[116–119]

For example, Guo et al. fabricated a wearable transient pressure sensor based on MXene nanosheets to detect radial muscle contraction and other physiological signals such as wrist pulse (Figure 7G, H). The fabrication process was as follows: tissue papers were immersed into MXene nanosheet solution with different concentrations to get MXene/tissue paper firstly. Next, the obtained MXene/tissue paper was deposited onto the PLA film with interdigitated electrodes. Finally, the above device was covered with a thin black PLA sheet to get the pressure sensor. This wearable pressure sensor with high sensitivity possessed a low detection limit of 10.2 Pa, and the broad range up to 30 kPa. Besides, the response time was only 11 ms and the power consumption was low to 10–8W. After more than 10,000 cycles, the sensors demonstrated great reproducibility. It is worth noting that this sensor can be degradable because of the selected materials.[119]

## 5.2 | Bioimaging

The various physicochemical properties of 2D nanosheets, such as quantum size effects, intrinsic photothermal performance, element enhanced contrast, and effective loading of functional contrast agents (CAs) make diagnostic imaging possible, implying that they have the ability to improve the diagnostic-imaging performance.[120] Diagnostic imaging can predict tumor location and guide PTT, which includes photoacoustic imaging (PAI), magnetic resonance imaging (MRI), X-Ray computed tomography (CT) and luminescence imaging. During the photothermal therapy, multi-mode imaging is also introduced sometimes.[121–124]

### 5.2.1 | Photoacoustic imaging

PAI is an emerging technology based on the conversion of light energy to sound energy which can overcome the high scattering of optical photons in biological tissues by using the photoacoustic effect, thereby providing higher spatial resolution for living bodies and imaging for deeper tissues. The light absorbed by the molecules will generate a pressure jump caused by heat, that will generate ultrasonic waves, which will be received by the acoustic detector and form an image.[120] Generally speaking, the higher the photothermal conversion capability of the contrast agent, the stronger the PA signal generated. MXene has a strong absorption capacity and conversion efficiency for a broad spectrum of light due to its semi-metallic properties and localized surface plasmon resonance (LSPR) effect, which can act as an efficient contrast agent. For example, inspired by the collaborative/sequential treatment method of photon hot air therapy, Yin et al. proposed a new treatment method by constructing 2D core/shell-structured $Nb_2C$-MSNs-SNO composite nanosheets. The mesoporous silica layer was used to coat the surface of $Nb_2C$ nanosheets to obtain a photo-triggered thermogas-generating nanoreactor, in which the mesopores stored NO donor (S-nitrosothiol (RSNO)) and the core of $Nb_2C$ generated heat shock under second NIR bio-window (NIR-II) laser irradiation. After injecting 4T1 tumor-bearing mice with constructed $Nb_2C$-MSNs-SNO composite nanosheets intravenously and performing PA imaging at different time intervals, the effective tumor accumulation of $Nb_2C$ MSNs-SNO with high tumor contrast of PAI in vivo could be seen. Moreover, because $Nb_2C$–MSNs–SNO accumulated at the tumor site, the PA signal gradually increased with time past and reached a maximum at 8 hours after injection (Figure 8A). The results showed that the constructed $Nb_2C$-MSNs-SNO composite nanosheet can be used as an excellent PA contrast agent.[125]

### 5.2.2 | Magnetic resonance imaging

As a non-invasive imaging means, MRI technology has a good spatial resolution, high-soft tissue contrast and no ionizing radiation. Therefore, it is interesting to apply this technique to biological imaging, and varied kinds of contrast agents are designed for the further improvement of sensitivity to obtain images with abundant information.[126] Liu et al. constructed superparamagnetic two-dimensional $Ti_3C_2$ MXenes for apparently effective cancer treatment by growing superparamagnetic $Fe_3O_4$ nanocrystals in situ on the surface of $Ti_3C_2$ MXenes. The constructed $Ti_3C_2$-IONPs MXene composites showed a high T-2 relaxivity of 394.2 $mM^{-1}$ $s^{-1}$ and apparently efficient contrast-enhanced magnetic resonance imaging of tumors, making therapeutic guidance potential (Figure 8A). What's more, the obtained MXene composites possessed outstanding photothermal conversion efficiency (48.6%) to kill cancer cells and ablate tumor tissues in vitro and in vivo efficiently.[127]

### 5.2.3 | X-ray computed tomography

Because of the 3D tomography of anatomical structures based on differences in X-ray absorption between lesions and tissues, X-ray CT has been used in medical imaging modalities abroad, and X-Ray computed tomography contrast agent (CTCA) is usually a nanomaterial including high atomic number (Z) elements.[120] Liu et al. have proposed a new type of superparamagnetic MXene-based therapeutic nanoplatform on the basis of $Ta_4C_3$ MXene and its further surface-superparamagnetic iron-oxide modification ($Ta_4C_3$-IONP-SPs) composite MXenes) to treat breast cancer effectively. Using redox reaction to in situ grow superparamagnetic IONPs on the surface of $Ta_4C_3$ MXene obtained by exfoliation strategy. Due to the high atomic number and X-ray attenuation coefficient of the Ta component in $Ta_4C_3$-IONP-SPs, they exhibited contrast-enhanced CT imaging performance. (Figure 8C), and the integrated IONPs were used as outstanding contrast agents for T-2-weighted MRI. Moreover, the $Ta_4C_3$-IONP-SPs composite nanosheets possessed high photothermal-conversion efficiency (32.5%) and eradicated tumor completely without reoccurrence.[14]

### 5.2.4 | Luminescence imaging

MXene-derived QDs possess unique properties such as stability of chemical and photo, high dispersibility, and photoluminescence properties that are tunable via changing the size, shape, or modification of the synthesized QDs. In

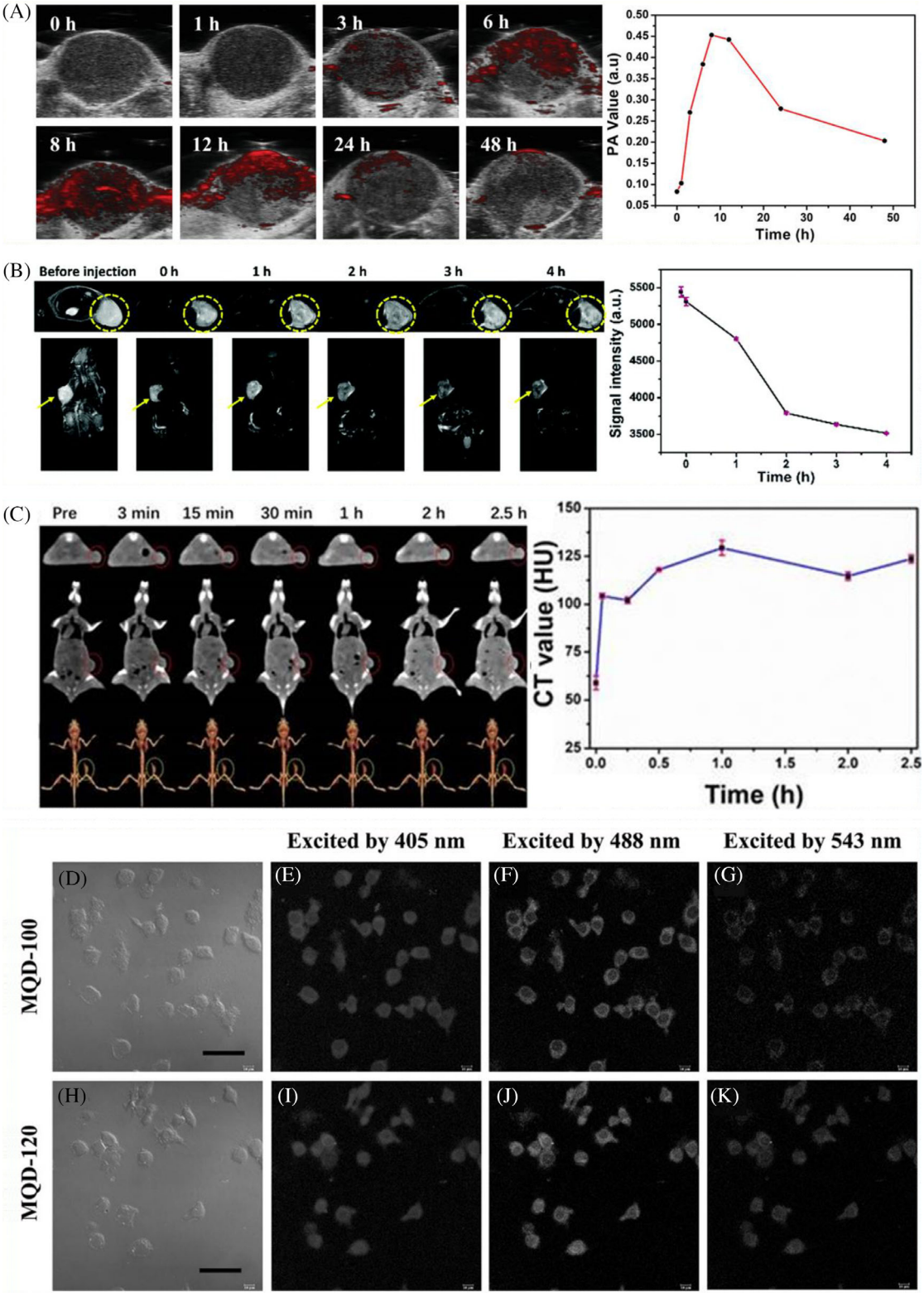


**FIGURE 8** MXenes for bioimaging. A, After intravenous injection with $Nb_2C$–MSNs–SNO, PA images in vivo and corresponding signal intensities of tumor were showed. Reproduced with permission.[125] Copyright 2020, Wiley. B, Before and after intravenously injection with $Ti_3C_2$–IONPs–SPs, transverse, coronal section and corresponding signal intensities of the T2-weighted MRI of 4T1 tumor-bearing mice were showed. Reproduced with permission.[127] Copyright 2018, Royal Society of Chemistry. C, The left picture showed transverse, coronal and 3D-rendering CT images of 4T1 tumor-bearing mouse, while the right picture demonstrated time-dependent CT values after intravenously injecting with $Ta_4C_3$-IONP-SPs. In which the red circles mark the tumor sites. Reproduced with permission.[14] Copyright 2018, Ivyspring International Publisher. (D-K) Bright-field and confocal imaging of RAW264.7 cells were showed. Reproduced with permission.[128] Copyright 2017, Wiley

2017, Xue et al. prepared monolayered $Ti_3C_2$ MQDs, which can be dissolved in water through a simple hydrothermal method. The choice of reaction temperature can control the average size of the MQDs. Because the obtained MQDs had strong quantum confinement, the PL spectra which was dependent on excitation was showed and the quantum yields was around 10%. RAW 264.7 cell labeling indicated that MQDs can be a candidate for biocompatible multicolor cellular imaging probe (Figure 8D-K). Besides, the as-prepared MQDs can detect $Zn^{2+}$ ions with high selectivity.[128]

## 5.3 | Tissue engineering

Compared with other biomedical applications, such as bioimaging, tumor treatment, antibacterial, etc. MXenes have fewer applications in tissue engineering. The application of MXene in tissue engineering includes bone tissue engineering,[76,129–132] skin tissue engineering,[15] nerve tissue engineering,[133,134] and myocardial tissue engineering[135,136] mainly.

Chen et al. designed a robust method to prepare strong and biocompatible $Ti_3C_2T_z$-enhanced poly lactic acid (PLA) nanocomposite membranes utilizing n-octyltriethoxysilane (OTES) as interfacial mediation. The ultimate tensile strength (UTS) of the OTES-$Ti_3C_2T_z$/PLA nanocomposite membranes was highly enhanced because of the strong interaction between OTES-$Ti_3C_2T_z$ and PLA. What's more, the addition of these $Ti_3C_2T_z$ nanosheets offered outstanding biocompatibility, such as improved proliferation, cell adhesion and osteogenic differentiation, which was beneficial to bone generation (Figure 9A-E).[130] Then, in order to evaluate the biocompatibility, osteo-inducibility, and guided bone regeneration ability of $Ti_3C_2T_x$ MXene in vitro and vivo, Zhang et al. prepared a multilayer $Ti_3C_2T_x$ MXene membrane. The obtained results from the experiments showed that $Ti_3C_2T_x$ MXene membrane has a high degree of cell compatibility and enhances osteogenic differentiation in vitro. When implanted in the subcutaneous part and skull defect of rats, the MXene membrane showed good biocompatibility, osteoinductivity and bone regeneration activity in vivo.[132]

Slow wound healing may lead to bacteria and fungi infection. Bacterial cellulose (BC)/$Ti_3C_2$ electroactive composite hydrogel was obtained via blending bacterial cellulose sol with $Ti_3C_2$ and crosslinking with trichloroethane by Mao et al. The research results show that the composite hydrogel has good biocompatibility and electrical conductivity, thus, can be used to induce cell adhesion, growth and proliferation through cell co-culture and electrical stimulation coupling, providing theory and experimental basis to promote the directed repair and regeneration of skin.[15]

About nerve tissue engineering, Nicolette et al. proposed a method of constructing $Ti_3C_2$ based flexible microelectrode. Owing to the high conductivity and specific surface area of the $Ti_3C_2$ MXene films, flexible arrays of $Ti_3C_2$ MXene microelectrodes have significantly low impedance with the ability to record neuronal activity in an accurate and sensitive way. In the article, a novel method for micropatterning $Ti_3C_2$ MXene into microelectrode arrays on flexible polymeric substrates was described and their use for in vivo micro-electrocorticography recording was outlined. The method can simply be extended to create MXene electrode arrays of arbitrary size or geometry for many other applications in bioelectronics and it can be suitable for use with other conductive inks besides $Ti_3C_2$ MXene. This method makes fabrication of microelectrodes from solution-based conductive inks facile and scalable, and especially allows harnessing the unique properties of hydrophilic $Ti_3C_2$ MXene to conquer a large number of the obstacles that have impeded the universal utilization of carbon-based nanomaterials for high-fidelity neural microelectrodes.[133] In addition, Nicolette et al. constructed $Ti_3C_2$ neuroelectronic devices through a high-throughput microfabrication process. The interface impedance of $Ti_3C_2$ electrode was reduced by four times compared with gold microelectrodes of the same size. What's more, $Ti_3C_2$ electrodes demonstrated a higher signal-to-noise ratio, lower baseline noise, and decreased sensitivity to 60 Hz interference compared with gold electrodes. According to the results of neuronal biocompatibility studies, neurons cultured on $Ti_3C_2$ are as viable as control cultured neurons. Besides, they have the ability to adhere, grow axons, and form functional networks. In a word, $Ti_3C_2$ MXene microelectrodes can be a candidate for strong platform technology for the purpose of high-resolution biological interfaces (Figure 9F-H).[137]

In addition, Ye et al. integrated mussel-inspired dopamine and conductive MXene $Ti_2C$ with hydrophilicity and biocompatibility into poly (ethylene glycol) diacrylate (PEGDA)-Gel- methacrylic anhydride (MA) cryogel to construct a bio-functional engineered cardiac patches (ECP) which had the ability to repair myocardial infarction (MI) when closing to natural heart in 2020. The production process is as follows: firstly, dispersing the MXene $Ti_2C$ obtained by the etching method into the prepolymer composed with dopamine-N′, N′-methylene-bisacrylamide, methacrylate-gelatin, and poly (ethylene glycol) diacrylate through facile water bath sonication evenly. After chemical cryogelation, a kind of resilient conductive $Ti_2C$-cryogel was obtained. The ECP with conductivity was assessed in vitro and implanted into MI rat model for MI treatment (Figure 9I). In vitro, a

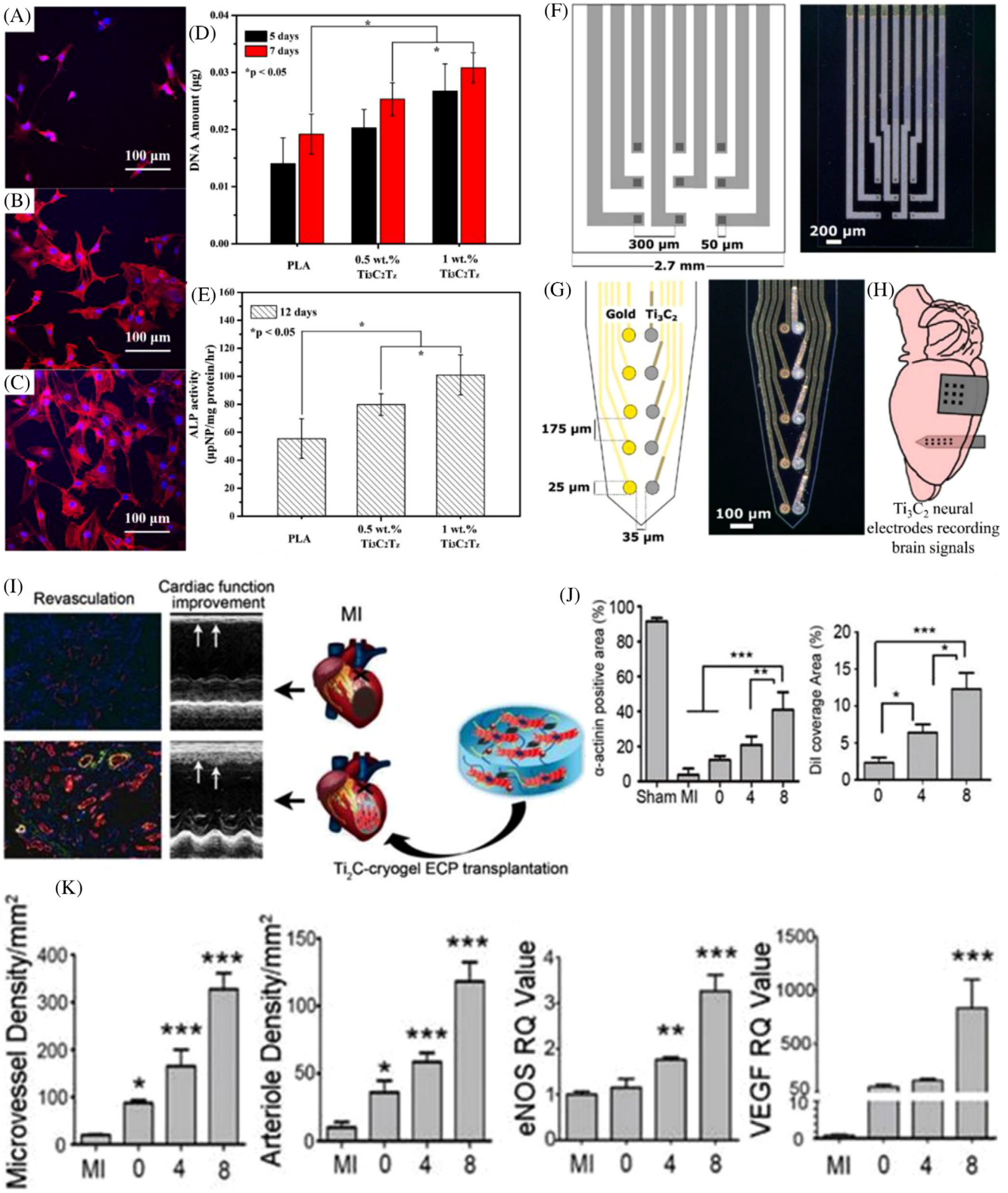


**FIGURE 9** MXenes for tissue engineering. (A-C) CLSM image of MC3T3-E1 cells adhered to pure PLA and OTES-$Ti_3C_2T_x$/PLA nanocomposite film. D, DNA assay to measure cell viability. E, ALP analysis to determine cell differentiation. Reproduced with permission.[130] Copyright 2018, Elsevier. (F-G) Schematics and bright-field microscopy image of $Ti_3C_2$ micro-ECoG array and $Ti_3C_2$/Au intracortical electrode array. H, Application of $Ti_3C_2$ arrays for neural recording at varied locations in the rat brain. Reproduced with permission.[137] Copyright 2018, American Chemical Society. I, Application of $Ti_2C$-cryogel in a rat MI model. J, In the infarcted heart, revasculation was encouraged by $Ti_2C$-cryogel ECP. K, The polarization of unrepaired M2 macrophage was induced by $Ti_2C$-cryogel ECP in MI region. Reproduced with permission.[136] Copyright 2020, Ivyspring International Publisher

3D vascular-like skeleton was seen in $Ti_2C$-8 cryogels inoculated with rat aortic endothelial cells. Clearly arranged sarcomeres and original insertion disc between mature CMs were formed after co-culturing $Ti_2C$ cryogel with cardiomyocytes (CM) for 7 days. The fabricated $Ti_2C$-8-cryogel ECP also showed fast calcium transients and synchronized tissue-like beats. Transplantation of $Ti_2C$-8-cryogel ECP into the infarcted heart of MI rat model can enhance heart function, decrease infarct size and hinder inflammation. The obvious vasoconstriction was also found, especially the newly formed small arteries (Figure 9J, K).[136]

## 5.4 | Antibacterial

The antibacterial mechanism of MXenes can be attributed to its semiconductor properties, good electrical conductivity, and hydrophilicity, oxygen-containing functional groups on the surface, atomic layer thickness, and optical properties such as the LSPR effect. Kashif et al. found that $Ti_3C_2T_x$ in colloidal aqueous solution can inhibit the growth of Gram (-) E. coli and Gram (+) Bacillus subtilis which was strongly dependent on the dose of MXenes and exceeded antibacterial activity of GO. Based on the various tests, it was found that the antimicrobial mechanism of $Ti_3C_2T_x$ MXene nanosheets can be related to the direct contact between $Ti_3C_2T_x$ MXene and the cell membrane, which destroyed cellular membranes and made cells die eventually. Another reason may be that $Ti_3C_2T_x$ nanosheets with strong reducing activity, reactive surface and the smallest size penetrated into microbial cells through direct physical penetration or endocytosis, which may cause $Ti_3C_2T_x$ to interact with certain molecules in the microbial cell walls and cytoplasm and lead to the disruption of cell structure and death of microorganism eventually.[67] Also, because the negatively charged $Ti_3C_2$ nanosheets had surface anionic properties, a conductive bridge will be formed on the insulating lipid bilayer, which promoted the transfer of electrons from bacterial cell components to the external environment, thereby causing cell death. In addition, similar to GO nanosheets, there is a reason to trust that the hydrogen bonds formed between the oxygen-containing groups on the surface of $Ti_3C_2T_x$ MXene and the lipopolysaccharide string in the cell membrane may inhibit bacterial growth.[67] Subsequently, Ahmad Arabi et al. verified that the antibacterial activity of the MXene nanosheets is related to size and exposure time. Besides, the quantitative analysis from flow cytometry, complementary technology and fluorescence imaging showed that the smallest nanosheets possessed the highest antibacterial activity against both Gram-negative and Gram-positive bacteria. What's more, the growth kinetics measurements indicated that the direct physical interaction between sharp edges of the nanosheets and the surface of the bacterial membrane is critical to the antibacterial properties (Figure 10A).[138] The production of reactive oxygen species (ROS) stimulated by MXenes was also a possible mechanism of bactericidal effect. Rajavel et al. determined the produced intracellular ROS levels upon exposure to MXenes through a 2′7′-dichlorodihydrofluorescein diacetate (H2DCFDA) kit. Intracellular ROS levels suggested that MXenes have the ability to hinder the activity of antioxidant enzymes and makethe ROS accumulate inside the bacterial cells which caused oxidative damage to biomacromolecules and cell membranes. Since superoxide dismutase (SOD) is an important defense enzyme against oxidation under stress conditions, the oxidative damage induced by MXenes was further assessed via analyzing SOD. The reduction of SOD activity demonstrates that the MXenes treatments damage the antioxidative system and could lead to the elevated intracellular ROS level and the final oxidative damage.[139] Recently, Feng et al. fabricated a stable titanium carbide@cuprous oxide (Ag @ $Ti_3C_2$ @ $Cu_2O$) nanocomposite with reducibility through a facile wet chemical method, which also had high-efficiency photocatalysis antibacterial activity. Besides, it had excellent antibacterial activity against Pseudomonas aeruginosa and Staphylococcus aureus. The electron-hole recombination efficiency of nanocomposites was analyzed by characterizing photoluminescence spectra. It was found that the charge transfer channel endowed by the heterostructure between nanocomposites greatly enhanced the efficiency of charge transfer and separation. Also, the life span of active electrons was prolonged and the generation of electrons was encouraged. (Figure 10B).[140]

## 5.5 | Therapeutics

### 5.5.1 | Photothermal therapy

So far, cancer is still one of the main threats to human life and health worldwide. Traditional surgical treatment will cause large wounds to the human body, and be prone to infection and recurrence. Besides, chemotherapy will cause not only the death of cancer cells, but also the death of normal cells. Recently, as an emerging minimally invasive treatment method with fewer by-sides, PTT is to ablate tumor cells by absorbing near-infrared light at the tumor site and converting it into heat. Because of larger surface area, higher photothermal conversion efficiency, surface with hydrophilicity and plentiful functional groups, MXenes have been widely studied for photothermal treatment of tumors. In addition, MXenes can also be used as a carrier for anticancer drugs and

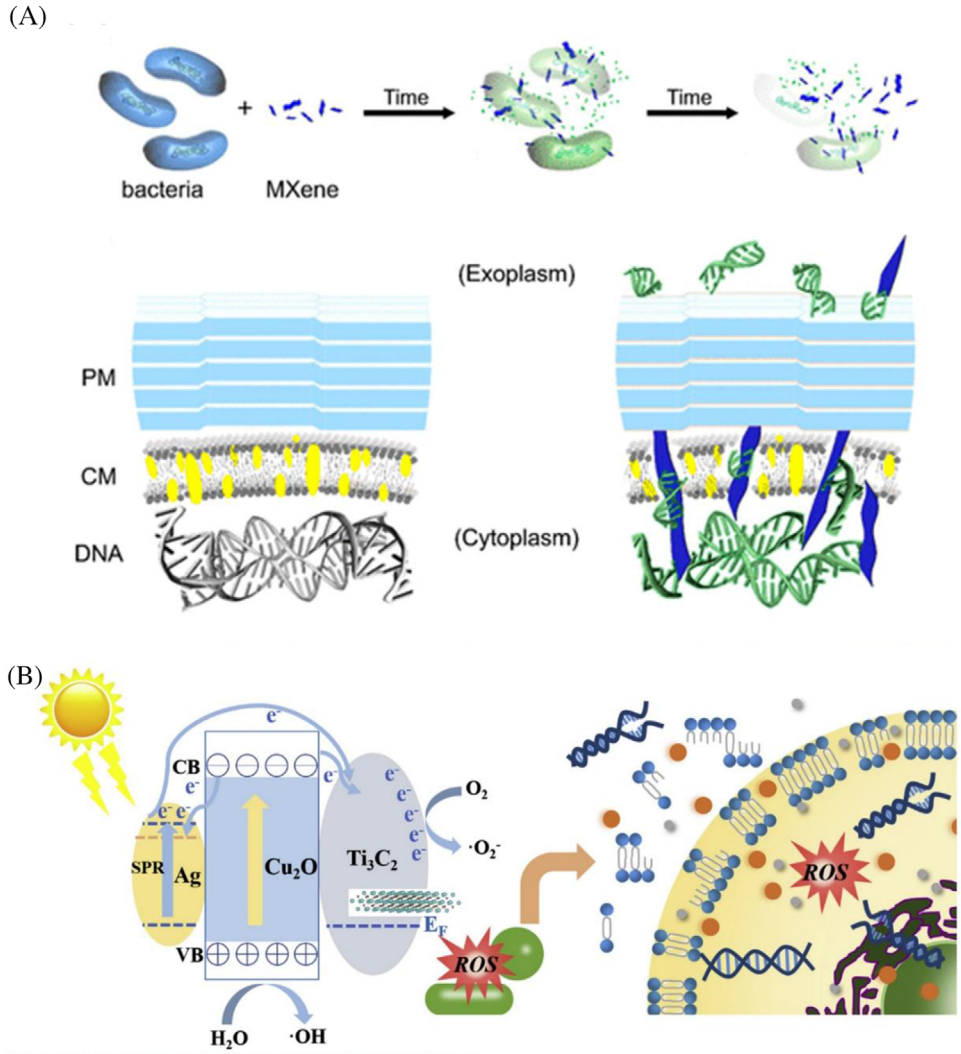


**FIGURE 10** MXenes for antibacterial. A, Schematic illustration of proposed antibacterial MoA of $Ti_3C_2T_x$ nanosheets. (PM: peptidoglycan mesh; CM: cytoplasmic membrane.) Reproduced with permission.[138] Copyright 2018, American Chemical Society. B, Schematic illustration of structure, energy band, electron-hole separation and the antibacterial mechanism of $Ag@Ti_3C_2@Cu_2O$. Reproduced with permission.[140] Copyright 2020, Elsevier

contrast agents for bioimaging to deliver drugs and monitor the process of treatment. These synergistic effects greatly increase the success rate of cancer treatment and bring cancer treatment convenient. The efficiency of PTT in vivo largely depends on the depth of tumor tissue or the depth of laser penetration, the accumulation of photothermal agents (PTAs) and their photothermal conversion efficiency, photoexcitation time, and optical power density. Lin et al. demonstrated for the first time that MXenes nanosheets with atomic thickness were used for photothermal ablation of cancer. Not only intravenous injection of $Ti_3C_2$ nanosheets modified with SP, but also local tumor implantation of phase-changeable poly (lactic-co-glycolic acid) (PLGA)/$Ti_3C_2$ organic-inorganic hybrid showed high photothermal conversion efficiency and photothermal ablation of tumor in vitro/in vivo (Figure 11A-C).[12] In addition, MXene can also cooperate with photodynamic and chemical treatment to for the purpose of killing and destruction of tumor cells. For instance, Liu et al. fabricated ultrathin $Ti_3C_2$ MXene by adding $Al^{3+}$ to avoid the loss of Al. The obtained nanosheets with excellent mass extinction coefficient (28.6 $Lg^{-1}$ $cm^{-1}$ at 808 nm), outstanding photothermal conversion efficiency (~58.3%) and effective singlet oxygen generation could be used as photothermal/photodynamic agents to treat cancer under 808 nm laser irradiation. After modifying MXenes with doxorubicin hydrochloride (DOX) and HA through a layer-by-layer way, the obtained MXenes with enhanced biocompatibility accumulated at the tumor site specifically, and released drug in a stimuli-responsive behavior, thus killing cancer cell effectively and destroying tumor tissue by photothermal/photodynamic/chemo

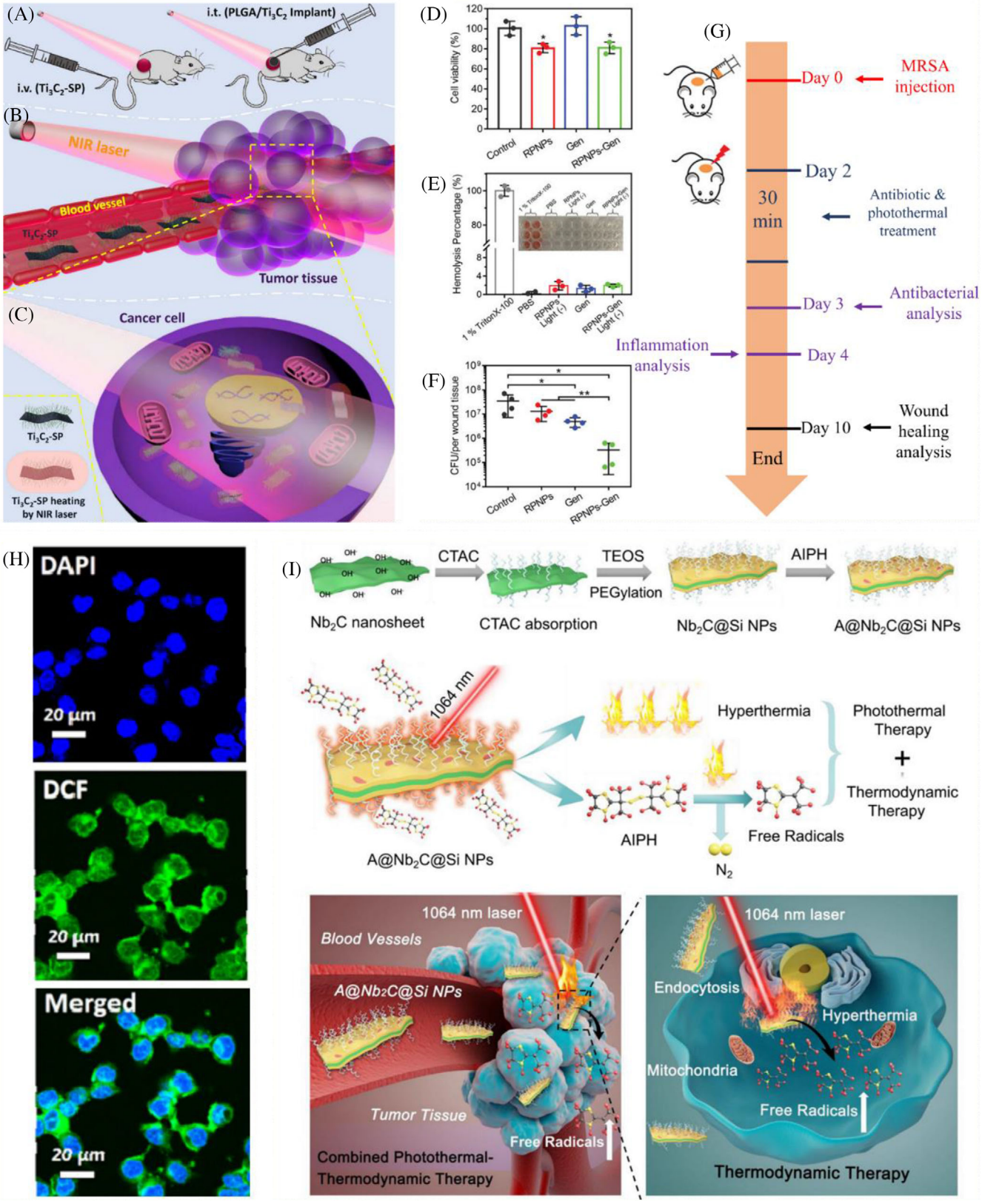


**FIGURE 11** MXenes for therapeutic application. A, $Ti_3C_2$–SP nanosheets were injected intravenously and phase-changeable PLGA/$Ti_3C_2$ implant was injected into the tumor. B, The $Ti_3C_2$–SP nanosheets arrived and accumulated at tumor tissues through EPR effect after intravenous injection. C, When $Ti_3C_2$–SP was exposed to NIR laser, the photothermal ablation of cancer cell happens. Reproduced with permission.[12] Copyright 2017, American Chemical Society. D, Cell viability of NIH-3T3 cells under light. E, Hemolysis percentage of samples and the corresponding images. F, CFU of MRSA in each wound tissue. G, Schematic of the combinatorial therapy protocol. Reproduced with permission.[143] Copyright

synergistic therapy.[141] In order to guide the photothermal ablation of the tumor to achieve better effect of tumor treatment, Dai et al. constructed $Ta_4C_3$ MXene-based composite nanosheets for multiple imaging-guided photothermal tumor ablation. The redox reaction activated on the surface of $Ta_4C_3$ MXene was used to grow $MnO_x$ nanoparticles in situ on the reduced surface of nanosheets which served as the high-performance contrast agents for contrast-enhanced CT.[124] In order to solve the problems of harsh synthesis conditions of $V_2C$ and low photothermal conversion efficiency (PTCE) in PPT, Shah et al. reported a green layering method that uses an algae extraction layer to intercalate for the production of high-volume (90%) large amounts of $V_2C$ nanosheets (NSs). The resulting $V_2C$ NSs possessed good structural integrity and excellent absorption in the NIR region with PTCE up to 48%. In addition, $V_2C$ NSs can be used as an effective PTA for PTT guided by PA and MRI.[142]

Apart from tumor ablation, PTT can also be used to stimulate multi-drug resistant bacteria to re-sensitize conventional antibiotics to achieve the purpose of antibacterial. Tan et al. made methicillin-resistant staphylococcus aureus (MRSA) sensitive to traditional aminoglycoside antibiotics again utilizing a low-temperature photothermal treatment (PTT, 45 degrees C) with red phosphorus nanoparticles. The proteomic technique and molecular dynamics (MD) simulation were used to prove that the PTT with low temperature had the ability to potentiate aminoglycoside antibiotics against MRSA selectively and the active sites of aspartic acid (ASP) residues in 2-aminoglycoside phosphotransferase (APH [2 '']) were thermally unstable. By detecting the consumption of adenosine triphosphate (ATP) in the catalytic reaction, it was found that the catalytic activity of the APH (2'')-a modified enzyme was significantly inhibited. While the prevention of the deprotonating process for the target -OH of gentamycin can inhibit its catalytic ability. In summary, the cooperative therapy showed apparently biocompatibility and treated MRSA infections successfully in vivo (Figure 11D-G).[143]

### 5.5.2 | Photodynamic therapy (PDT)

Similar to photothermal therapy, PDT is an effective and non-invasive treatment strategy. Due to the electrical and optical properties of MXenes, they can be used as photosensitizers in PDT to activate ROS through photochemical methods and the activated ROS can cause damage to tumor cells. So far, there have been fewer studies of MXenes on PDT than PTT, while most MXenes-based PDT is combined with PTT to synergistically treat cancer. In Figure 11H, 2′,7′-dichlorofluorescein diacetate (DCFH-DA) was used as a probe to detect the generation of ROS in cells under 808 nm laser irradiation (0.8 W $cm^{-2}$, 10 minutes). The bright green fluorescence of DCF in cells indicated that $Ti_3C_2$-DOX generated ROS of high levels intracellular when hyaluronidase (HAase) degraded the HA shell to disclose the active surface of $Ti_3C_2$ nanosheets.[141] Although the mechanism of MXenes' ROS generation is not clear yet, it is speculated from the photodynamic behavior of black phosphorus and graphene quantum dots that the production of $^1O_2$ may be owing to the energy transfer of photo-excited electrons from $Ti_3C_2$ to triplet oxygen (ground oxygen, $^3O_2$). In addition, based on earlier reports, the ability of metals (especially gold nanoparticles) to generate ROS under visible light irradiation depends on their LSPR effect, so the LSPR effect of transition metal-containing MXenes may be also a reason in generating $^1O_2$, while the large surface area of MXene nanosheet probably leads to the enhanced LSPR.[144]

### 5.5.3 | Thermodynamic therapy

Since the tumor microenvironment is an oxygen-deficient microenvironment, it may be unfavorable for some treatment methods that require oxygen. For example, an oxygen-deficient environment may hinder the production of reactive oxygen species. Therefore, Xiang et al presented a method using thermodynamics to treat cancer, which took advantage of free radicals generated by thermally unstable initiators that have nothing to do with oxygen to kill cancer cells. The construction process of the photon/thermal responsive hybrid nano-system was as follows: coating the surface of 2D $Nb_2C$ MXene nanosheets with mesoporous silica layers for versatility, then the thermal decomposition initiator (AIPH) is effectively loaded into the mesopores to control the generation/release of free radicals. When exposed to 1064 nm NIR-II laser irradiation, the photothermal effect of $Nb_2C$ @ $mSiO_2$ NP made the encapsulated AIPH release and free radicals generated. Under normal and low oxygen content, the same lethal effect on cancer cells was showed. At the same time, the treatment process can be monitored by interesting

2020, Wiley. H, Fluorescence image of ROS detected in cells. Reproduced with permission.[141] Copyright 2017, American Chemical Society. I, The thermodynamic therapy caused by the free radicals generated by the thermal decomposition of AIPH was combined with the photothermal therapy of AIPH @ $Nb_2C$ @ $mSiO_2$ NP under light. Reproduced with permission.[145] Copyright 2019, American Chemical Society

multi-peak fluorescence, PA and photothermal imaging. In addition, after injection of AIPH @ $Nb_2C$ @ $mSiO_2$ NPs for 6 hours and 12 hours, the strong fluorescent signal mainly gathered in the liver, kidney and tumor site. The seizure of mononuclear macrophages may cause AIPH @ $Nb_2C$ @ $mSiO_2$ / Cy5.5 NP accumulate in the liver, the fluorescent signal in the kidney may be due to the possible renal excretion, and the aggregation in the tumor site was owing to the enhanced EPR effect most likely. Pharmacokinetic studies had shown that the extended cycle time was also consistent with the biodistribution results greatly. According to the results of in vivo toxicity studies, the constructed AIPH @ $Nb_2C$ @ $mSiO_2$ nanoplatform has high biosecurity and biocompatibility (Figure 11I).[145]

## 5.6 | Drug delivery system

Common methods of cancer treatment include surgery, chemotherapy and radiotherapy with the anticancer drugs such as cisplatin, methotrexate cytarabine, paclitaxel, and doxorubicin. However, not only do most anticancer drugs have cytotoxic effects on cancer cells, they also cause harm to non-malignant cells of the human body. Therefore, the slow and controlled release of drugs has become a major research focus in cancer chemotherapy. As an emerging branch of 2D nanomaterials, MXenes have aroused great interest in using them as drug carriers due to their planar structure, rich surface functional groups, biocompatibility and negatively charged surface. Although nanosized $Ti_3C_2$ which is the first MXene for drug delivery vehicles has an EPR effect and can accumulate at the tumor site, it needs to be surface-modified because it restacks under physiological conditions. The tumor microenvironment has a lower pH than the physiological microenvironment of normal tissues. In view of this, a controlled release nanoplatform can be designed for the reason that the presence of $H^+$ will destroy the electrostatic interaction between the drug and MXene. In addition, the controlled release of the drug can also be achieved through the stimulation of near-infrared radiation.

For example, Liu et al. used MXene $Ti_3C_2$ with a negatively charged surface to interact with DOX as a cationic model drug, and prepared a nanoplatform based on $Ti_3C_2$ nanosheets ($Ti_3C_2$-DOX) through layer-by-layer adsorption, where $Ti_3C_2$ acted as a carrier for cationic anticancer drugs and the load is up to 84.2%. Coating nanosheets with HA improves biocompatibility and enables the system to actively target $CD44^+$ overexpressing tumor cells, and also effectively prevents DOX from being released under neutral conditions. Because of the laser-induced photothermal effect of $Ti_3C_2$ (about 50°C), DOX released due to the destruction of electrostatic interactions in the $Ti_3C_2$-DOX system. All in all, $Ti_3C_2$-DOX has high responsiveness to light and heat, pH and enzymes (Figure 12A).[141] However, due to the limitations and lack of surface chemistry, Han et al. constructed a distinct "therapeutic mesopore" layer onto the surface of 2D $Nb_2C$ MXene through versatile sol-gel chemistry. First, the surfactant with positive charges cetyltrimethylammonium chloride (CTAC) was introduced into the surface of $Nb_2C$ MXenes through electrostatic interaction. Next, an organic silica source (tetraethyl orthosilicate, TEOS) was added to the reaction system, and its hydrolyzed/condensed oligomer was further self-assembled with surfactant micelles, thereby forming mesoporous silica shells on the surface of 2D $Nb_2C$ MXenes. The positively charged surfactant is retained in the mesopore as a mesopore-forming agent and can be directly used as a drug molecule to effectively kill cancer cells, besides, the synthesized mesopores can be almost completely filled with surfactants in the shape of self-assembled micelles which led to the high drug loading (32.57%). In addition, there was a large amount of salt chemistry on the surface of composite nanosheets, which makes further surface engineering be possible. The use of PEGylation ensures that these nanosheets possessed high stability in the physiological environment. The composite nanosheets conjugated with arginine-glycine-aspartic (RGD) peptides can recognize and bind integrin $\alpha v\beta 3$ overexpressed on cancer cell membranes specifically (Figure 12B). Besides, the constructed nanotherapeutic platform showed high light-to-heat conversion capacity ($\eta$: 28.6%), which can treat cancer with a combination of chemotherapy and PTT.[13] Later, for the first time, a composite hydrogel based on cellulose and $Ti_3C_2$ MXene with fast response near-infrared stimuli was synthesized by Xing et al. When the anticancer drug DOX is loaded (84% drug loading), cellulose/MXene hydrogel can significantly accelerate the release of DOX under irradiation, which may be due to the hole expansion that was triggered by 808 nm light irradiation three-dimensional cellulose-based network (Figure 12C).[146]

# 6 | CYTOCOMPATIBILITY AND CYTOTOXICITY EVALUATIONS OF MXENES

So far, there are not many studies on the cytotoxicity of the original MXenes, which are very important to biomedical applications. Nasrallah et al. used a zebrafish embryo model to investigate the biocompatibility of $Ti_3C_2T_x$ via assessing its potential toxicity in vivo (Figure 13A-D). Since the amount of $Ti_3C_2T_x$ attached/absorbed is proportional to the concentration of titanium, the content

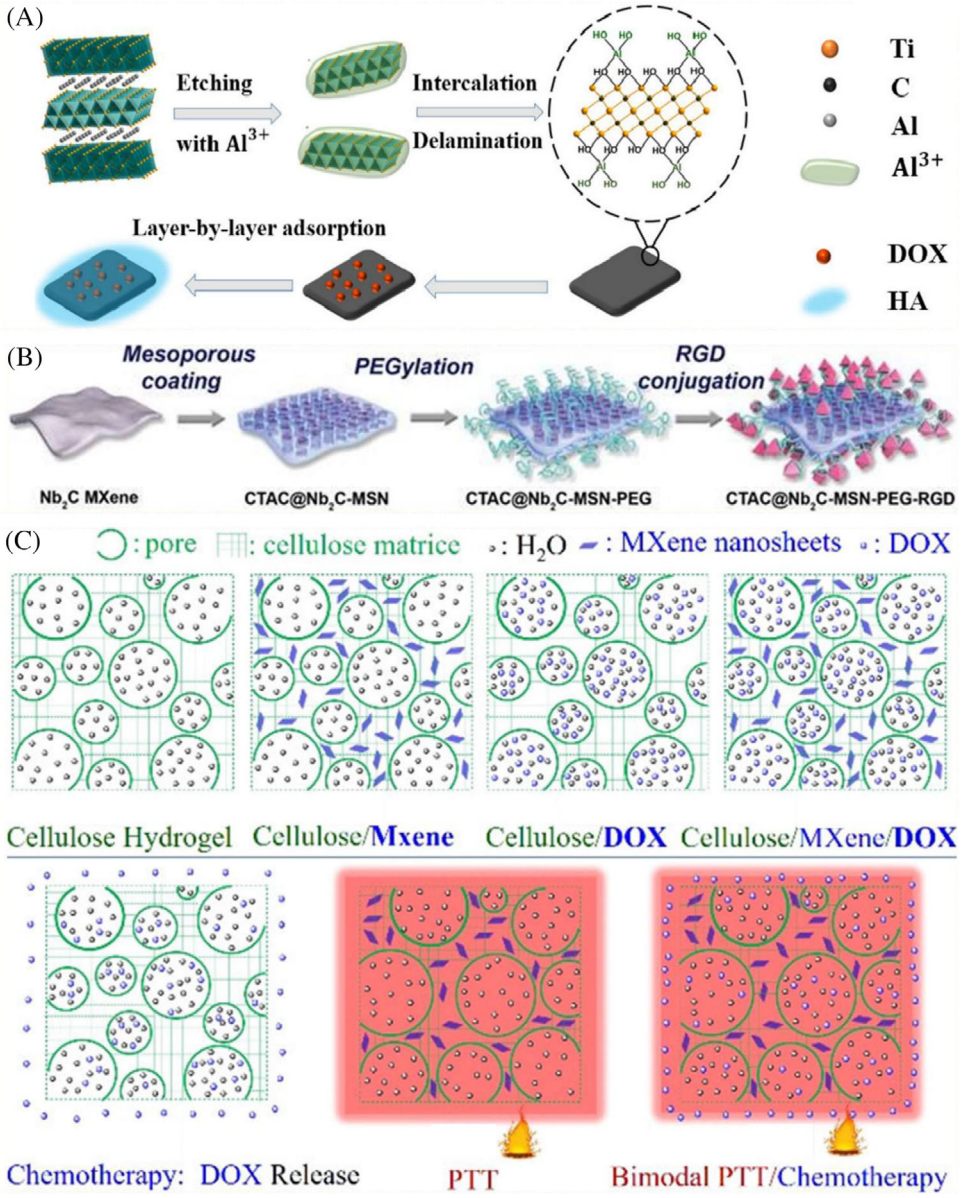


**FIGURE 12** MXenes for drug delivery. A, Scheme of the fabrication of $Ti_3C_2$-Based Nanoplatform through layer-by-layer absorption. Reproduced with permission.[141] Copyright 2017, American Chemical Society. B, The synthesis and surface modification process of CTAC @ $Nb_2C$-MSN. Reproduced with permission.[13] Copyright 2018, Ivyspring International Publisher. C, Four kinds of cellulose-based hydrogels and release of hydrogel under different conditions. Reproduced with permission.[146] Copyright 2018, American Chemical Society

of titanium attached/absorbed in the zebrafish embryo was determined by inductively coupled plasma mass spectrometry (ICP-MS) to find that the titanium content is related to the dose. Acute toxicity assessment indicates when the concentrations of nanosheet reached above 25 μM, the nanosheets aggregated around the embryos, which further indicated that 100 μg $mL^{-1}$ $Ti_3C_2T_x$ resulted in very marginal acute toxicity. Besides, the lethal concentration 50 ($LC_{50}$) values of the MXenes were over 257.5 μg $mL^{-1}$ at 96 hours, this result showed values of "practically non-toxicity" with an $LC_{50}$ of more than 100 μg $mL^{-1}$ based on the Acute Toxicity Rating Scale by the Fish and Wildlife Service (FWS). In addition, their effects on motor behavior and the nervous system have been studied. Neurotoxicity and exercise measurements showed that the embryos treated with $Ti_3C_2T_x$ had normal movement behavior, and the quantity of neurons in the spinal cord area was roughly equal to the amount observed in dimethyl sulfoxide (DMSO) negative controls, indicating that the no observed effect concentration (NOEC) dose (50 μg $mL^{-1}$) of $Ti_3C_2T_x$ nanosheets had no effect on embryonic neurons and muscle activity. All results showed that in a homogeneous solution, $Ti_3C_2T_x$ of 100 μM was non-toxic. However, the exposure of embryos to $Ti_3C_2T_x$ at concentrations over

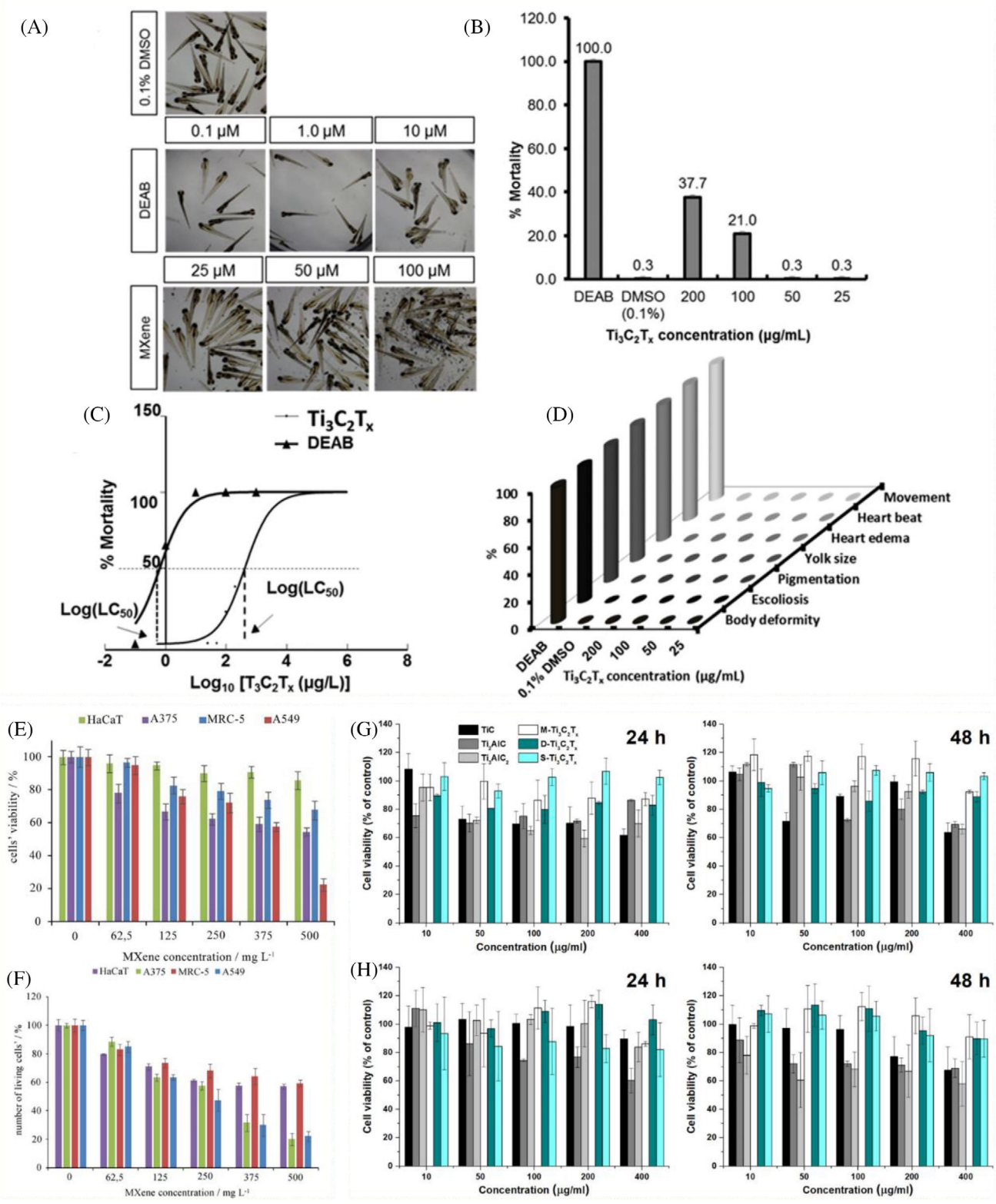


**FIGURE 13** Cytocompatibility and cytotoxicity evaluations of MXenes. A, Pictures about acute toxicity under varied treatment condition. B, Percentages of the cumulative mortality. C, Mortality response curve of DEAB and $Ti_3C_2T_x$. $LC_{50}$(Ti-NP) = 257.5 μg $mL^{-1}$. D, Teratogenic phenotype analysis of $Ti_3C_2T_x$ under varied concentrations compared with the controls. Reproduced with permission.[147] Copyright 2018, Royal Society of Chemistry. E, The results of MTT assay. F, The results of calcein-AM assay. Reproduced with permission.[148] Copyright 2017, Elsevier. G, The percentage of tetrazolium salt reduced to formazan was calculated with reference to untreated control cells. Reproduced with permission.[149] Copyright 2019, American Society of Chemistry

100 μM had very little teratogenic effects. The observation of the lowest observed effect concentration (LOEC) with mortality of 21% at 96 hours may be due to the large volume of $Ti_3C_2T_x$ aggregated into the embryo which could not be tolerated, bound and destroyed the embryo's cell membrane. Large aggregates may cause sudden blockage of capillaries in the vascular system, especially the presence of capillaries in the heart which leads to severe sudden death at a specific time.[147]

And Jastrzebska et al. used two normal (MRC-5 and HaCaT) and two cancerous (A549 and A375) cell lines to study the biological activity of 2D $Ti_3C_2$ MXene nanosheets. From the results of calcein-AM assay and MTT assay, the viability of normal cells and cancer cells decreases with the concentration of MXenes increasing, but the viability of cancer cells declines faster than normal cells. And, when the concentration of MXenes is lower than about 125 mg $L^{-1}$, the survival rate of normal cells can reach more than about 70%. Speculation about the mechanism of toxicity may be that the MXenes stimulated the production of ROS (Figure 13E, F).[148] Later in 2019, Scheibe et al. fabricated $Ti_3C_2T_x$ with many, few and single layers besides TiC, $Ti_2AlC$ and $Ti_3AlC_2$. Then the human fibroblasts (MSU1.1) and cervical cancer cells (HeLa) were used as model cells to investigate and compare the biological effect of prepared MXenes. The results indicated that higher concentrations (≥400 μg/mL) of TiC, $Ti_2AlC$, and $Ti_3AlC_2$ particles with sizes < 44 μm could be damaging to the cells because of oxidative and mechanical stress. The $Ti_3C_2T_x$ with all forms showed safety to MSU1.1 cell and only the $Ti_3C_2T_x$ with the highest concentration demonstrated insignificant cytotoxicity. Also, the cytotoxicity was dependent on the type of cells, and there were fewer living cells in the cancer origin (Figure 13G, H).[149]

## 7 | CONCLUSIONS AND PERSPECTIVE

As a new 2D material, MXenes have arisen great interest owing to their unique properties: semiconductor properties, electrical properties such as electrocatalysis and LSPR effect, magnetic properties, mechanical properties, atomic layer thickness, biocompatibility, large specific surface area and various surface functional groups. The structure, properties, synthetic methods, surface functionalization, biomedical applications and cytotoxicity evaluation of MXenes are summarized in this review. Although MXenes have made some achievements in antibacterial therapy, biological imaging, photothermal therapy, sensors for biomedical applications, photodynamic therapy, tissue engineering and other fields, there are still many problems of MXenes to be solved.

First of all, as a new 2D material with great prospects in biomedical applications, there are only a few reports on the biocompatibility of MXenes where most of the studies on biocompatibility Ti-based MXenes. However, the cell uptake behavior of MXenes-based materials and the impact of their surface functionalization on biocompatibility are important for most biomedical applications. Therefore, more efforts should be put into the investigation of long-term toxicity, biocompatibility, pharmacokinetics and biodistribution of MXenes in small animal models and large animal models. It may be considered to study the biocompatibility of MXenes by category, for example the biocompatibility of this class of MXenes based on Ti. In addition, their impacts on the ecological environment should be considered.

Up to now, most of the synthetic strategies of MXenes are top-down methods, which will introduce more impurities and have insufficient control over experiments and products, while only a few people are studying the bottom-up methods that can synthesize controllable products. Therefore, more efforts should be made to explore more synthetic methods, realize large-scale synthesis, expand the variety of MXenes family, and manufacture tunable MXenes with more properties. For example, some physical etching methods such as reactive ion etching, sputter etching, reactive ion beam etching can be selected. About the construction of drug delivery systems, since most of them are hydrophilic substances, MXenes and modifiers are bound by physical adsorption and non-covalent in most cases, which is difficult to achieve controlled release and unstable under extreme conditions. It is necessary to develop more innovative surface modification strategies so that the obtained composites can meet the requirements of various biomedical applications. For example, SIPGP and aryl diazonium chemistry can be considered to modify MXenes.

The researches on the performance of MXenes mainly focus on the electrical and optical properties so far, while the researches on their magnetic properties are less, and the applications extended by magnetic properties are less compared with the first two properties, especially the magnetic properties used in biomedical applications are even less, besides MRI imaging. What's more, some mechanisms of MXenes are still unclear, such as the mechanism of MXenes stimulating the production of ROS. A better understanding of the mechanism is conducive to optimizing materials, improving their properties and using them more appropriately. Also, more MXenes with unique structures can be explored. Some unique structures may improve the electron transmission capacity, increase the drug-carrying area and so on. Other two-dimensional materials can be considered to solve the above problems. For example, the antibacterial mechanism of $MoS_2$ can be referred to. Finally, more applications of MXenes should be explored in biomedical fields, such as acoustic dynamics therapy. Noting that two materials are

sometimes combined into composite materials to improve the total performance. However, the combination of two materials is not only a combination of advantages but also a combination of weakness, which is a problem worth considering.

## ACKNOWLEDGMENTS

The authors thanks for the support from the National Natural Science Foundation of China (61875015), the Science and Technology Planning Project of Guangdong Province (2018B030331001), the Beijing Natural Science Foundation (JQ20038), the National Youth Talent Support Program, and the Fundamental Research Funds for the Central Universities.

## ORCID

*Zhou Li* https://orcid.org/0000-0002-9952-7296

## REFERENCES

1. Y. Xie, H. Zhang, H. Huang, Z. Wang, Z. Xu, H. Zhao, Y. Wang, N. Chen, W. Yang, *Nano Energy* **2020**, *74*, 104928.
2. H. Huang, X. Chu, H. Su, H. Zhang, Y. Xie, W. Deng, N. Chen, F. Liu, H. Zhang, B. Gu, W. Deng, W. Yang, *J. Power Sources* **2019**, *415*, 1.
3. M. Ghidiu, M. R. Lukatskaya, M.-Q. Zhao, Y. Gogotsi, M. W. Barsoum, *Nature* **2014**, *516*, 78.
4. M. R. Lukatskaya, O. Mashtalir, C. E. Ren, Y. Dall'Agnese, P. Rozier, P. L. Taberna, M. Naguib, P. Simon, M. W. Barsoum, Y. Gogotsi, *Science* **2013**, *341*, 1502.
5. S. Cao, B. Shen, T. Tong, J. Fu, J. Yu, *Adv. Funct. Mater.* **2018**, *28*, 1800136.
6. Z. Guo, J. Zhou, L. Zhu, Z. Sun, *J. Mater. Chem. A* **2016**, *4*, 11446.
7. J. Zhang, Y. Zhao, X. Guo, C. Chen, C.-L. Dong, R.-S. Liu, C.-P. Han, Y. Li, Y. Gogotsi, G. Wang, *Nat. Catal.* **2018**, *1*, 985.
8. W.-T. Cao, C. Ma, D.-S. Mao, J. Zhang, M.-G. Ma, F. Chen, *Adv. Funct. Mater.* **2019**, *29*, 1905898.
9. W.-T. Cao, H. Ouyang, W. Xin, S. Chao, C. Ma, Z. Li, F. Chen, M.-G. Ma, *Adv. Funct. Mater.* **2020**, 2004181.
10. K. Wang, Z. Lou, L. Wang, L. Zhao, S. Zhao, D. Wang, W. Han, K. Jiang, G. Shen, *ACS Nano* **2019**, *13*, 9139.
11. D. Wang, L. Wang, Z. Lou, Y. Zheng, K. Wang, L. Zhao, W. Han, K. Jiang, G. Shen, *Nano Energy* **2020**, *78*, 105252.
12. H. Lin, X. Wang, L. Yu, Y. Chen, J. Shi, *NanoLett.* **2017**, *17*, 384.
13. X. Han, X. Jing, D. Yang, H. Lin, Z. Wang, H. Ran, P. Li, Y. Chen, *Theranostics* **2018**, *8*, 4491.
14. Z. Liu, H. Lin, M. Zhao, C. Dai, S. Zhang, W. Peng, Y. Chen, *Theranostics* **2018**, *8*, 1648.
15. L. Mao, S. Hu, Y. Gao, L. Wang, W. Zhao, L. Fu, H. Cheng, L. Xia, S. Xie, W. Ye, Z. Shi, G. Yang, *Adv. Healthc. Mater.* **2020**, *9*, 2000872.
16. M. Naguib, M. Kurtoglu, V. Presser, J. Lu, J. Niu, M. Heon, L. Hultman, Y. Gogotsi, M. W. Barsoum, *Adv. Mater.* **2011**, *23*, 4248.
17. M. Naguib, O. Mashtalir, J. Carle, V. Presser, J. Lu, L. Hultman, Y. Gogotsi, M. W. Barsoum, *ACS Nano* **2012**, *6*, 1322.
18. J. Halim, M. R. Lukatskaya, K. M. Cook, J. Lu, C. R. Smith, L.-Å. Näslund, S. J. May, L. Hultman, Y. Gogotsi, P. Eklund, M. W. Barsoum, *Chem. Mater.* **2014**, *26*, 2374.
19. A. Feng, Y. Yu, Y. Wang, F. Jiang, Y. Yu, L. Mi, L. Song, *Mater. Design* **2017**, *114*, 161.
20. P. Urbankowski, B. Anasori, T. Makaryan, D. Er, S. Kota, P. L. Walsh, M. Zhao, V. B. Shenoy, M. W. Barsoum, Y. Gogotsi, *Nanoscale* **2016**, *8*, 11385.
21. X. Sang, Y. Xie, M.-W. Lin, M. Alhabeb, K. L. Van Aken, Y. Gogotsi, P. R. C. Kent, K. Xiao, R. R. Unocic, *ACS Nano* **2016**, *10*, 9193.
22. M. Song, S.-Y. Pang, F. Guo, M.-C. Wong, J. Hao, *Adv. Sci.* **2020**, *7*, 2001546.
23. J. Zhou, X. Zha, X. Zhou, F. Chen, G. Gao, S. Wang, C. Shen, T. Chen, C. Zhi, P. Eklund, S. Du, J. Xue, W. Shi, Z. Chai, Q. Huang, *ACS Nano* **2017**, *11*, 3841.
24. S. Sun, J. Yang, X. Chen, W. Cui, J. Huang, T. Yang, Z. Zhang, Q. Wang, *ScriptaMater.* **2020**, *181*, 10.
25. G. Zhao, J. Chen, Y. Li, L. Zheng, J. Li, X. Wang, M. Li, *J. Eur. Ceram. Soc.* **2017**, *37*, 83.
26. J. Zhou, X. Zha, F. Y. Chen, Q. Ye, P. Eklund, S. Du, Q. Huang, *Angew. Chem. Inter. Ed.* **2016**, *55*, 5008.
27. J. Mei, G. A. Ayoko, C. Hu, J. M. Bell, Z. Sun, *Sustain. Mater. Techno.* **2020**, *25*, e00156.
28. L. Verger, C. Xu, V. Natu, H.-M. Cheng, W. Ren, M. W. Barsoum, *Curr. Opin. Solid St. M.* **2019**, *23*, 149.
29. C. Xu, L. Wang, Z. Liu, L. Chen, J. Guo, N. Kang, X.-L. Ma, H.-M. Cheng, W. Ren, *Nat. Mater.* **2015**, *14*, 1135.
30. M. Zeng, Y. Chen, J. Li, H. Xue, R. G. Mendes, J. Liu, T. Zhang, M. H. Rümmeli, L. Fu, *Nano Energy* **2017**, *33*, 356.
31. W. Sun, X. Wang, J. Feng, T. Li, Y. Huan, J. Qiao, L. He, D. Ma, *Nanotechnology* **2019**, *30*, 38.
32. F. Zhang, Z. Zhang, H. Wang, C. H. Chan, N. Y. Chan, X. X. Chen, J.-Y. Dai, *Phys. Rev. Mater.* **2017**, *1*, 034002.
33. X. Xiao, H. Yu, H. Jin, M. Wu, Y. Fang, J. Sun, Z. Hu, T. Li, J. Wu, L. Huang, Y. Gogotsi, J. Zhou, *ACS Nano* **2017**, *11*, 2180.
34. S. Joshi, Q. Wang, A. Puntambekar, V. Chakrapani, *ACS Energy Lett.* **2017**, *2*, 1257.
35. Z. Kang, Z. Zheng, H. Wei, Z. Zhang, X. Tan, L. Xiong, T. Zhai, Y. Gao, *Sensors* **2019**, *19*, 1099.
36. Y. Gogotsi, B. Anasori, *ACS Nano* **2019**, *13*, 8491.
37. S. Zhao, W. Kang, J. Xue, *J. Mater. Chem. C* **2015**, *3*, 879.
38. S. Y. Pang, W. F. Io, L. W. Wong, J. Zhao, J. Hao, *Adv. Sci.* **2020**, *7*, 1903680.
39. K. Li, M. Liang, H. Wang, X. Wang, Y. Huang, J. Coelho, S. Pinilla, Y. Zhang, F. Qi, V. Nicolosi, Y. Xu, *Adv. Funct. Mater.* **2020**, 2000842.
40. K. Li, X. Wang, S. Li, P. Urbankowski, J. Li, Y. Xu, Y. Gogotsi, *Small* **2020**, *16*, 1906851.
41. S. A. Shah, T. Habib, H. Gao, P. Gao, W. Sun, M. J. Green, M. Radovic, *Chem. Commun.* **2017**, *53*, 400.
42. L. Wang, H. Liu, X. Lv, G. Cui, G. Gu, *J. Alloy. Compd.* **2020**, *828*, 154251.
43. H. Shi, M. Yue, C. J. Zhang, Y. Dong, P. Lu, S. Zheng, H. Huang, J. Chen, P. Wen, Z. Xu, Q. Zheng, X. Li, Y. Yu, Z.-S. Wu, *ACS Nano* **2020**, *14*, 8678.
44. J. Qin, L. Hao, X. Wang, Y. Jiang, X. Xie, R. Yang, M. Cao, *Chem.-Eur. J.* **2020**, *26*, 11231.
45. B. Shao, Z. Liu, G. Zeng, H. Wang, Q. Liang, Q. He, M. Cheng, C. Zhou, L. Jiang, B. Song, *J. Mater. Chem. A* **2020**, *8*, 7508.
46. Z. Guo, X. Zhu, S. Wang, C. Lei, Y. Huang, Z. Nie, S. Yao, *Nanoscale* **2018**, *10*, 19579.

47. X. Li, F. Liu, D. Huang, N. Xue, Y. Dang, M. Zhang, L. Zhang, B. Li, D. Liu, L. Wang, H. Liu, X. Tao, *Adv. Funct. Mater.* **2020**, *30*, 2000308.
48. F. Ran, T. Wang, S. Chen, Y. Liu, L. Shao, *Appl. Surf. Sci.* **2020**, *511*, 145627.
49. X. Jiang, A. V. Kuklin, A. Baev, Y. Ge, H. Ågren, H. Zhang, P. N. Prasad, *Phys. Rep.* **2020**, *848*, 1.
50. X. Han, J. Huang, H. Lin, Z. Wang, P. Li, Y. Chen, *Adv. Healthc. Mater.* **2018**, *7*, 1701394.
51. G. Ying, S. Kota, A. D. Dillon, A. T. Fafarman, M. W. Barsoum, *Flat. Chem.* **2018**, *8*, 25.
52. K. Hantanasirisakul, M.-Q. Zhao, P. Urbankowski, J. Halim, B. Anasori, S. Kota, C. E. Ren, M. W. Barsoum, Y. Gogotsi, *Adv. Electron. Mater.* **2016**, *2*, 1600050.
53. H. Kim, Z. Wang, H. N. Alshareef, *Nano Energy* **2019**, *60*, 179.
54. H. Zhang, G. Yang, X. Zuo, H. Tang, Q. Yang, G. Li, *J. Mater. Chem. A* **2016**, *4*, 12913.
55. R. Momeni Feili, M. Dadsetani, R. Nejatipour, A. Ebrahimian, *J. Electron. Mater.* **2020**, *49*, 2502.
56. M. Naguib, V. N. Mochalin, M. W. Barsoum, Y. Gogotsi, *Adv. Mater.* **2014**, *26*, 992.
57. J. Yang, X. Luo, S. Zhang, L. Chen, *Phys. Chem. Chem. Phys.* **2016**, *18*, 12914.
58. H. Hadipour, Y. Yekta, *Phys. Rev. B* **2019**, *100*, 195118.
59. Z. Jing, H. Wang, X. Feng, B. Xiao, Y. Ding, K. Wu, Y. Cheng, *J. Phys. Chem. Lett.* **2019**, *10*, 5721.
60. M. Iqbal, J. Fatheema, Q. Noor, M. Rani, M. Mumtaz, R. K. Zheng, S. A. Khan, S. Rizwan, *Mater. Today Chem.* **2020**, *16*, 100271.
61. S. Zhong, B. Xu, A. Cui, S. Li, S. Liao, G. Wang, G. Liu, B. Sun, *ACS Omega* **2020**, *5*, 864.
62. P. Lv, Y.-L. Li, J.-F. Wang, *Phys. Chem. Chem. Phys.* **2020**, *22*, 11266.
63. X. Li, X. Yin, S. Liang, M. Li, L. Cheng, L. Zhang, *Carbon* **2019**, *146*, 210.
64. R. M. Ronchi, J. T. Arantes, S. F. Santos, *Ceram. Int.* **2019**, *45*, 18167.
65. K. Chen, N. Qiu, Q. Deng, M.-H. Kang, H. Yang, J.-U. Baek, Y.-H. Koh, S. Du, Q. Huang, H.-E. Kim, *ACS Biomater. Sci. Eng.* **2017**, *3*, 2293.
66. B. Xu, M. Zhu, W. Zhang, X. Zhen, Z. Pei, Q. Xue, C. Zhi, P. Shi, *Adv. Mater.* **2016**, *28*, 3333.
67. K. Rasool, M. Helal, A. Ali, C. E. Ren, Y. Gogotsi, K. A. Mahmoud, *ACS Nano* **2016**, *10*, 3674.
68. Z. Guo, J. Zhou, C. Si, Z. Sun, *Phys. Chem. Chem. Phys.* **2015**, *17*, 15348.
69. J. Cao, Z. Zhou, Q. Song, K. Chen, G. Su, T. Zhou, Z. Zheng, C. Lu, X. Zhang, *ACS Nano* **2020**, *14*, 7055.
70. F. Bu, M. M. Zagho, Y. Ibrahim, B. Ma, A. Elzatahry, D. Zhao, *Nano Today* **2020**, *30*, 100803.
71. H. Huang, R. Jiang, Y. Feng, H. Ouyang, N. Zhou, X. Zhang, Y. Wei, *Nanoscale* **2020**, *12*, 1325.
72. P. Zhang, L. Wang, Z. Huang, J. Yu, Z. Li, H. Deng, T. Yin, L. Yuan, J. K. Gibson, L. Mei, L. Zheng, H. Wang, Z. Chai, W. Shi, *ACS Appl. Mater. Inter.* **2020**, *12*, 15579.
73. R. Liang, Y. Li, M. Huo, H. Lin, Y. Chen, *ACS Appl. Mater. Inter.* **2019**, *11*, 42917.
74. C. Ding, J. Liang, Z. Zhou, Y. Li, W. Peng, G. Zhang, F. Zhang, X. Fan, *Chem. Eng. J.* **2019**, *378*, 122205.
75. J. Chen, K. Chen, D. Tong, Y. Huang, J. Zhang, J. Xue, Q. Huang, T. Chen, *Chem. Commun.* **2015**, *51*, 314.
76. Q. Yang, H. Yin, T. Xu, D. Zhu, J. Yin, Y. Chen, X. Yu, J. Gao, C. Zhang, Y. Chen, Y. Gao, *Small* **2020**, *16*, 1906814.
77. F. Wang, C. Yang, M. Duan, Y. Tang, J. Zhu, *Biosens. Bioelectron.* **2015**, *74*, 1022.
78. F. Wang, M. Cao, Y. Qin, J. Zhu, L. Wang, Y. Tang, *RSC Adv.* **2016**, *6*, 88934.
79. F. Wang, Z. Wang, J. Zhu, H. Yang, X. Chen, L. Wang, C. Yang, *J. Mater. Sci.* **2017**, *52*, 3556.
80. Y. Zhang, B. Guo, L. Hu, Q. Xu, Y. Li, D. Liu, M. Xu, *J. Alloy. Compd.* **2018**, *732*, 448.
81. Y. Zhang, R. Zhan, Q. Xu, H. Liu, M. Tao, Y. Luo, S. Bao, C. Li, M. Xu, *Chem. Eng. J.* **2019**, *357*, 220.
82. D. Shan, J. He, L. Deng, S. Yan, H. Luo, S. Huang, Y. Xu, *Results Phys.* **2019**, *15*, 102750.
83. Q. Xue, Z. Pei, Y. Huang, M. Zhu, Z. Tang, H. Li, Y. Huang, N. Li, H. Zhang, C. Zhi, *J. Mater. Chem. A* **2017**, *5*, 20818.
84. M. Mohammadniaei, A. Koyappayil, Y. Sun, J. Min, M. H. Lee, *Biosens. Bioelectron.* **2020**, *159*, 112208.
85. R. P. Pandey, K. Rasool, V. E. Madhavan, B. Aissa, Y. Gogotsi, K. A. Mahmoud, *J. Mater. Chem. A* **2018**, *6*, 3522.
86. J. Zheng, B. Wang, A. Ding, B. Weng, J. Chen, *J. Electroanal. Chem.* **2018**, *816*, 189.
87. R. Tang, S. Zhou, C. Li, R. Chen, L. Zhang, Z. Zhang, L. Yin, *Adv. Funct. Mater.* **2020**, *30*, 2000637.
88. Y. He, L. Ma, L. Zhou, G. Liu, Y. Jiang, J. Gao, *Nanomaterials* **2020**, *10*, 866.
89. S. M. George, B. Kandasubramanian, *Ceram. Int.* **2020**, *46*, 8522.
90. F. Wang, C. Yang, C. Duan, D. Xiao, Y. Tang, J. Zhu, *J. Electrochem. Soc.* **2015**, *162*, B16.
91. G. Wang, J. Sun, Y. Yao, X. An, H. Zhang, G. Chu, S. Jiang, Y. Guo, X. Sun, Y. Liu, *Food Anal. Meth.* **2020**, *13*, 420.
92. F. Duan, C. Guo, M. Hu, Y. Song, M. Wang, L. He, Z. Zhang, R. Pettinari, L. Zhou, *Actuat. B-Chem.* **2020**, *310*, 127844.
93. L. Liu, Y. Wei, S. Jiao, S. Zhu, X. Liu, *Biosens. Bioelectron.* **2019**, *137*, 45.
94. S. Hroncekova, T. Bertok, M. Hires, E. Jane, L. Lorencova, A. Vikartovska, A. Tanvir, P. Kasak, J. Tkac, *Processes* **2020**, *8*, 580.
95. H. Wang, J. Sun, L. Lu, X. Yang, J. Xia, F. Zhang, Z. Wang, *Anal. Chim. Acta.* **2020**, *1094*, 18.
96. S. Kumar, Y. Lei, N. H. Alshareef, M. A. Quevedo-Lopez, K. N. Salama, *Biosens. Bioelectron.* **2018**, *121*, 243.
97. S. Zhou, C. Gu, Z. Li, L. Yang, L. He, M. Wang, X. Huang, N. Zhou, Z. Zhang, *Appl. Surf. Sci.* **2019**, *498*, 143889.
98. H. Liu, C. Duan, C. Yang, W. Shen, F. Wang, Z. Zhu, *Sensor. Actuat. B-Chem.* **2015**, *218*, 60.
99. Y. Lei, A. H. Alshareef, W. Zhao, S. Inal, *ACS Appl. Nano Mater.* **2020**, *3*, 1166.
100. H. L. Chia, C. C. Mayorga-Martinez, N. Antonatos, Z. Sofer, J. J. Gonzalez-Julian, R. D. Webster, M. Pumera, *Anal. Chem.* **2020**, *92*, 2452.
101. H. Gu, Y. Xing, P. Xiong, H. Tang, C. Li, S. Chen, R. Zeng, K. Han, G. Shi, *ACS Appl. Nano Mater.* **2019**, *2*, 6537.
102. Y. Lei, W. Zhao, Y. Zhang, Q. Jiang, J.-H. He, A. Baeumner, O. S. Wolfbeis, Z. L. Wang, K. N. Salama, H. N. Aishareef, *Small* **2019**, *15*, 1901190.
103. R. B. Rakhi, P. Nayak, C. Xia, H. N. Alshareef, *Sci. Rep.* **2016**, *6*, 36422.

104. F. Zhao, Y. Yao, C. Jiang, Y. Shao, D. Barcelo, Y. Ying, J. Ping, *J. Hazard. Mater.* **2020**, *384*, 121358.
105. D. Song, X. Jiang, Y. Li, X. Lu, S. Luan, Y. Wang, Y. Li, F. Gao, *J. Hazard. Mater.* **2019**, *373*, 367.
106. Y. Jiang, X. Zhang, L. Pei, S. Yue, L. Ma, L. Zhou, Z. Huang, Y. He, J. Gao, *Chem. Eng. J.* **2018**, *339*, 547.
107. L. Zhou, X. Zhang, L. Ma, J. Gao, Y. Jiang, *Biochem. Eng. J.* **2017**, *128*, 243.
108. H. Li, Y. Wen, X. Zhu, J. Wang, L. Zhang, B. Sun, *ACS Sustain. Chem. Eng.* **2020**, *8*, 520.
109. S. S. Shankar, R. M. Shereema, R. B. Rakhi, *ACS Appl. Mater. Inter.* **2018**, *10*, 43343.
110. P. A. Rasheed, R. P. Pandey, K. A. Jabbar, J. Ponraj, K. A. Mahmoud, *Anal. Methods.* **2019**, *11*, 3851.
111. F. Shahzad, A. Iqbal, S. A. Zaidi, S.-W. Hwang, C. M. Koo, *J. Ind. Eng. Chem.* **2019**, *79*, 338.
112. H. Zhang, Z. Wang, Q. Zhang, F. Wang, Y. Liu, *Biosens. Bioelectron.* **2019**, *124*, 184.
113. Q. Wu, N. Li, Y. Wang, Y. Liu, Y. Xu, S. Wei, J. Wu, G. Jia, X. Fang, F. Chen, X. Cui, *Biosens. Bioelectron.* **2019**, *144*, 111697.
114. Y. Li, Z. Kang, L. Kong, H. Shi, Y. Zhang, M. Cui, D. Yang, *Mat. Sci. Eng. C* **2019**, *104*, 110000.
115. G. Cai, Z. Yu, P. Tong, D. Tang, *Nanoscale* **2019**, *11*, 15659.
116. Y. Ma, Y. Yue, H. Zhang, F. Cheng, W. Zhao, J. Rao, S. Luo, J. Wang, X. Jiang, Z. Liu, N. Liu, Y. Gao, *Acs Nano* **2018**, *12*, 3209.
117. Y. Ma, N. Liu, L. Li, X. Hu, Z. Zou, J. Wang, S. Luo, Y. Gao, *Nat. Commun.* **2017**, *8*, 1207.
118. Y. Cai, J. Shen, G. Ge, Y. Zhang, W. Jin, W. Huang, J. Shao, J. Yang, X. Dong, *Acs Nano* **2018**, *12*, 56.
119. Y. Guo, M. Zhong, Z. Fang, P. Wan, G. Yu, *Nano Lett.* **2019**, *19*, 1143.
120. H. Lin, Y. Chen, J. Shi, *Adv. Sci.* **2018**, *5*, 1800518.
121. Z. Xie, S. Chen, Y. Duo, Y. Zhu, T. Fan, Q. Zou, M. Qu, Z. Lin, J. Zhao, Y. Li, L. Liu, S. Bao, H. Chen, D. Fan, H. Zhang, *ACS Appl. Mater. Inter.* **2019**, *11*, 22129.
122. D.-Y. Zhang, H. Xu, T. He, M. R. Younis, L. Zeng, H. Liu, C. Jiang, J. Lin, P. Huang, *Nanoscale* **2020**, *12*, 7174.
123. Y. Cheng, F. Yang, G. Xiang, K. Zhang, Y. Cao, D. Wang, H. Dong, X. Zhang, *Nano Lett.* **2019**, *19*, 1179.
124. C. Dai, Y. Chen, X. Jing, L. Xiang, D. Yang, H. Lin, Z. Liu, X. Han, R. Wu, *ACS Nano* **2017**, *11*, 12696.
125. H. Yin, X. Guan, H. Lin, Y. Pu, Y. Fang, W. Yue, B. Zhou, Q. Wang, Y. Chen, H. Xu, *Adv. Sci.* **2020**, *7*, 1901954.
126. M. Soleymaniha, M. A. Shahbazi, A. R. Rafieerad, A. Maleki, A. Amiri, *Adv. Healthc. Mater.* **2019**, *8*, 1801137.
127. Z. Liu, M. Zhao, H. Lin, C. Dai, C. Ren, S. Zhang, W. Peng, Y. Chen, *J. Mater. Chem. B* **2018**, *6*, 3451.
128. Q. Xue, H. Zhang, M. Zhu, Z. Pei, H. Li, Z. Wang, Y. Huang, Y. Huang, Q. Deng, J. Zhou, S. Du, Q. Huang, C. Zhi, *Adv. Mater.* **2017**, *29*, 1604847.
129. G. P. Awasthi, B. Maharjan, S. Shrestha, D. P. Bhattarai, D. Yoon, C. H. Park, C. S. Kim, *Colloids Surf. A* **2020**, *586*, 124282.
130. K. Chen, Y. Chen, Q. Deng, S.-H. Jeong, T.-S. Jang, S. Du, H.-E. Kim, Q. Huang, C.-M. Han, *Mater. Lett.* **2018**, *229*, 114.
131. S. Pan, J. Yin, L. Yu, C. Zhang, Y. Zhu, Y. Gao, Y. Chen, *Adv. Sci.* **2020**, *7*, 1901511.
132. J. Zhang, Y. Fu, A. Mo, *Int. J. Nanomedicine* **2019**, *14*, 10091.
133. N. Driscoll, K. Maleski, A. G. Richardson, B. Murphy, B. Anasori, T. H. Lucas, Y. Gogotsi, F. Vitale, *J. Vis. Exp.* **2020**, *156*, e60741.
134. H. Rastin, B. Zhang, A. Mazinani, K. Hassan, J. Bi, T. T. Tung, D. Losic, *Nanoscale* **2020**, *12*, 16069.
135. A. Rafieerad, W. Yan, G. L. Sequiera, N. Sareen, E. Abu-El-Rub, M. Moudgil, S. Dhingra, *Adv. Healthc. Mater.* **2019**, *8*, 1900569.
136. G. Ye, Z. Wen, F. Wen, X. Song, L. Wang, C. Li, Y. He, S. Prakash, X. Qiu, *Theranostics* **2020**, *10*, 2047.
137. N. Driscoll, A. G. Richardson, K. Maleski, B. Anasori, O. Adewole, P. Lelyukh, L. Escobedo, D. K. Cullen, T. H. Lucas, Y. Gogotsi, F. Vitale, *ACS Nano* **2018**, *12*, 10419.
138. A. A. Shamsabadi, M. S. Gh, B. Anasori, M. Soroush, *ACS Sustain. Chem. Eng.* **2018**, *6*, 16586.
139. K. Rajavel, S. Shen, T. Ke, D. Lin, *2D Materials* **2019**, *6*, 035040.
140. H. Feng, W. Wang, M. Zhang, S. Zhu, Q. Wang, J. Liu, S. Chen, *Appl. Catal. B-Environ.* **2020**, *266*, 118609.
141. G. Liu, J. Zou, Q. Tang, X. Yang, Y. Zhang, Q. Zhang, W. Huang, P. Chen, J. Shao, X. Dong, *ACS Appl. Mater. Inter.* **2017**, *9*, 40077.
142. S. Zada, W. Dai, Z. Kai, H. Lu, X. Meng, Y. Zhang, Y. Cheng, F. Yan, P. Fu, X. Zhang, H. Dong, *Angew. Chem. Int. Edit.* **2020**, *132*, 6663.
143. L. Tan, Z. Zhou, X. Liu, J. Li, Y. Zheng, Z. Cui, X. Yang, Y. Liang, Z. Li, X. Feng, S. Zhu, K. W. K. Yeung, C. Yang, X. Wang, S. Wu, *Adv. Sci.* **2020**, *7*, 1902070.
144. K. Huang, Z. Li, J. Lin, G. Han, P. Huang, *Chem. Soc. Rev.* **2018**, *47*, 5109.
145. H. Xiang, H. Lin, L. Yu, Y. Chen, *ACS Nano* **2019**, *13*, 2223.
146. C. Xing, S. Chen, X. Liang, Q. Liu, M. Qu, Q. Zou, J. Li, H. Tan, L. Liu, D. Fan, H. Zhang, *ACS Appl. Mater. Inter.* **2018**, *10*, 27631.
147. G. K. Nasrallah, M. Al-Asmakh, K. Rasool, K. A. Mahmoud, *Environ. Sci. Nano* **2018**, *5*, 1002.
148. A. M. Jastrzebska, A. Szuplewska, T. Wojciechowski, M. Chudy, W. Ziemkowska, L. Chlubny, A. Rozmyslowska, A. Olszyna, *J. Hazard. Mater.* **2017**, *339*, 1.
149. B. Scheibe, J. K. Wychowaniec, M. Scheibe, B. Peplinska, M. Jarek, G. Nowaczyk, L. Przysiecka, *ACS Biomater. Sci. Eng.* **2019**, *5*, 6557.

**How to cite this article:** Huang J, Li Z, Mao Y, Li Z. Progress and biomedical applications of MXenes. *Nano Select*. 2021;1-29.
https://doi.org/10.1002/nano.202000309